Response to reviewers

We would like to thank the reviewers for their comments. Note that based on comments from the reviewers, we have simplified and made the numerical experiments more uniform. First, the thickness of the level ice is 2 m for all the experiments. Second, the viscous coefficients (see eq. 5 and 6 in the revised manuscript) are always capped using the approach of Hibler 1979. Finally, the numerical approach was slightly modified: we seek the steady-state solution of $\rho h \partial u/\partial t = \nabla \cdot \sigma$. instead of solving directly $\nabla \cdot \sigma = 0$. Although both approaches give the same answer, the new one is more consistent with the stability analysis described in the appendix. Because of these changes, all the numerical experiments were redone.

Reviewers 2 and 3 both had comments about mechanical closing of the lead behind the ship and that this should depend on the pressure at the boundaries (larger pressure should cause a shorter lead). To address these comments we have done additional experiments and added a new figure (Fig. 11). For the experiments of Fig.11, it is assumed that the length of the lead behind the ship decreases linearly as the pressure at the boundaries increases. Interestingly, we find that over a notable range of pressure applied at the boundaries, the maximum pressure on the ship does not vary much. This is a consequence of compensating effects: a larger pressure at the boundaries causes the lead to be shorter which decreases the stress concentration in the vicinity of the ship, making the maximum pressure weakly sensitive to the pressure at the boundary.

Below, the comments from the reviewers (1) are in normal character. Our responses (2) are in bold while changes to the manuscript (3) mentioned here are also in bold and in quotes.

REVIEWER 1

(1) I think this paper is well-written, presents important new results on the downscaling of pack ice pressure in models for application to ships in ice, and should

be accepted with only the following minor revision.

On Figures 4 and 5, panel (c): can the authors please specify what type of distribution was fitted to the data, provide the distribution parameters, and the 95% confidence intervals of the distribution parameters?

(2) Figures 4 and 5 are figures 3 and 4 in the revised manuscript. These figures show the probability density functions (PDF) calculated from the simulated 2D fields of pressure. There is no fit to the model outputs. The curves simply show the value of the PDF for all the bins (the bin size is 0.25 kNm^{-1}). We have added the following text when introducing figure 3:

(3) "From these simulated 2D pressure fields, probability density functions (PDF) are calculated using bins of 0.25 kNm^{-1}. They are shown in Fig. 3c which further demonstrates that the simulated fields are very similar at 10 and 20 m resolutions."

REVIEWER 2

(1) The work is correctly done, but it may be a little overly enthusiastic in applying the conclusions of the analysis to ship operations in ice. The problem analysed in the paper is one in engineering; the stress field around a void and/or inclusion in a large plate under stress. A ship moving through an ice field under pressure is a much more complex problem.

(2) We agree. Note, however, that we do not consider the case of a ship moving through sea ice but only the case of a ship beset in heavy sea ice conditions. Note that we have added the following sentence in the introduction of the revised manuscript:

(3) "In contrast with studies mentioned in the last paragraph, we focus on ship besetting, rather than on a ship progressing in an ice covered

region. We also study the downscaling of sea ice pressure from the km scale to scales relevant for navigation activities (tens of m).”

(1) The work merits publication but the conclusion that the ship creates a stress concentration by breaking a channel might be couched in a more conditional manner. Experience generally shows that if the channel does not close, the ship is experiencing little or no pressure. The rate of channel closing and closing distance is proportional to the ice pressure that the ship feels. A longer open channel behind the ship is an indication of lower ice pressure, not higher.

(2) We understand what the reviewer means here. But our point of view is that a ship beset might have a lead (i.e., a channel still open) behind it and that it is unclear what is the length of this lead. The numerical experiments with the ship should be seen as a sensitivity study about the impact of the lead length and ice conditions in the lead (which are unknowns). For the same large-scale pressure at the boundaries, we argue that the pressure on the ship should decrease as the lead closes (either thermodynamically or mechanically) behind the ship.

(2) To address this comment by the reviewer we have added an additional experiment for which it is assumed that the length of the lead decreases linearly as the large-scale pressure prescribed at the boundaries increases. This is described in subsection 6.2 and the results shown in a new figure (Fig. 11).

(1) Some specific corrections, improvements or comments:

(1) Larger font on some of the plots in figures would help readability.

(2) We have reworked and improved all the figures.

(1) For Fig. 1 add the surface wind scale to panel b).

(2) The reference vector is on the island on the lower-right side of the small domain.

(1) Line 51; the author should be Loset?

(2) Yes. It has been corrected.

(1) Line 175; would it complicate Fig. 2 to also show Mi and Mc on it?

(2) We have decided to simplify the way the digitized ship is defined. The ship is defined by land cells. The boundary conditions are no slip and no outflow. This is explained in the description of the experimental setup (section 3 in the revised manuscript). The masks Mi and Mc are not required anymore. Note that this leads to results qualitatively the same and allows us to draw the same conclusion.

(1) Line 211; Figure 4 a) and b) look very similar to results of finite element analysis of an elastic plate with a crack or void.

(1) Line 113; stress concentration at the tips of the lead and zero normal pressure on the boundary of the lead translate to the maximum and minimum pressures in Figure 4 c). I looks like the probability is greater than 1 for pressure 10 kN/m, check the y-axis scale. For the 10 m grid size the 28 cells that border on the lead versus the 5122 - 40 cells in the ice field give a 28 / 262104 (1.07e-04) probability of zero pressure. This doesnt seem to agree with Fig. 4 c).

(2) This is due to the fact that we use small bins (of 0.25 $\mathbf{kNm^{-1}}$) and show the probability density not the probability. For figures 3 and 4, we have verified that the sum of the PDF times the bin width is indeed 1.0.

(1) Figure 5 presents results of experiments with refrozen lead and ridged ice in

addition to the 1 km lead. Not surprising is the result that there is no change of zero stress on the lead boundary or stress concentration at the tips of the lead. It seems that doubling the ice thickness from 1 to 2 m, Figure 4 versus Figure 5, the maximum stress at the tip of the leads is increased. Any explanation? Is it fair to compare maximum pressure in Fig. 6 b) with P* = 20 kN/m2 for a 1 km long lead with Figure 5. Both are for 2 m ice thickness.

(2) For both figures the thickness of the level ice is 2 m. The confusion is due to the fact that the validation experiment done just before the one for Fig. 4 was conducted with a constant thickness of 1 m. To improve the clarity of the manuscript, that experiment was redone with a thickness of 2 m. In fact, the thickness of the level ice is 2 m for all the experiments of the revised manuscript. Fig. 4 and Fig. 5 (Fig. 3 and Fig. 4 in the revised manuscript) do not show the same maximum pressure because the leads do not have the same width.

(1) For Figure 8 add a label to the x-axes, resolution and units of m. The maximum pressure of Figure 8 a) agrees with that in Figure 5 c), about 38 kN/m in both cases.

(2) Done.

(1) The pressure field in Figure 9 seems reasonable given that a relatively stiff object (the ship) is placed at one end of a long cavity (lead). Your analysis only considers pressures, the ice also deforms and the further from the tip of the crack (lead) the greater the closing of the lead and thus higher lateral pressure.

(2) We agree. The limitations of our experimental setup are discussed in the conclusion of the revised manscript.

(1) The results presented in Figures 9 and 10 are quite consistent with the analysis model of a stiff object (ship) at the end of an elongated cavity (lead) in a more compliant medium (ice field). The results are consistent with stress analy-

sis around inclusions. The analysis is correct, but it may be premature to draw conclusions about applying the results to operation of a ship in pressured ice.

(2) We have added a few sentences in the conclusion to describe the limitations of our numerical setup.

(1) There is literature in the Arctic engineering field that considers scale effect of ice pressures. The authors could look to this literature as they continue working in this field. See for example;

Sanderson, T.J.O., 1988. Ice Mechanics Risks to Offshore Structures. Graham and Trotman, London, UK. Croasdale, K.

Croasdale, K.R., 2009. Limit force ice loads - an update. Proceedings 20th POAC Conference, Paper POAC09-030, Lulea, Sweden.

(2) We thank the reviewer for these references.

REVIEWER 3

(1) The paper documents the development of an idealised sub-climate model grid cell (5kmx5km) modelling study of the sea ice internal pressures found at the tips of leads. A viscous plastic model is used to find the immediate internal stress states across the model for given internal stress states at the model domain boundaries. A single lead is placed within the sea ice of arbitrary size in the form of a rectangle of no ice and the stress states at the tips of the lead are documented. An idealised ship is placed at the end of the simulated lead and the simulated ice pressures on the ship are recorded. Model simulations are documented showing the changing ice stresses for a number of cases. First the model is tested for the case of no-ship, with the expected deformation rates related to an analytical case. Cases with leads of various sizes and for various model resolutions are also tested.

(1) Additional ice features are also added to the domain, showing that the shape

of the largest lead is the controlling factor for the highest ice pressures in the model. A ship is then positioned at the end of the largest lead and the stresses upon the ship are documented. Multiple experiments are performed varying the lead length (and also introducing a refrozen sea surface to the lead), ice strength parameter and the compressive and shear strengths of the ship itself. The authors conclude that the defects within a sub climate model grid cell are the greatest controller of sea ice pressure. They lead this conclusion to suggest that the pressure stress on a beset ship at the end of a lead of its own making will reduce as the lead surface consolidates. I can see how the results in this paper will help inform the navigation of ice covered seas.

(1) The paper is in general very well written and the introduction and description are easy to follow. I suggest that is published with some additional explanations. Also the title of the paper should be changed to reflect the specific situation that is being simulated.

(1) Improvements can be made to text in the form of overall motivation of the study. Explicitly saying in the introduction and methods and results that aim of the paper is to focus on the increased ice pressure at the tip of a lead where a ship is likely to be present would be a beneficial addition to the paper. Also the paper needs to clearly state that this study models a single instantaneous stress field for a particular setup. This limitation also needs to be addressed in the conclusions when the case of lead closure is discussed.

(2) The motivation of the study was improved/clarified in the revised manuscript. We have also changed the title of the paper (see below). To address the reviewer's comment about the instantaneous stress field, we have added the following sentence in section 3:

(3) "Our numerical simulations therefore provide 2D static fields of the internal stresses inside this small domain."

(1) Whilst the authors mention that waiting for a lead to consolidate will reduce

the stress on the ship, how likely is it that the lead will close mechanically before then?

(2) Reviewer 2 had a similar comment. There is certainly mechanical closure but it is difficult to estimate the length of the lead for a certain large-scale pressure applied at the boundaries. This is why Fig. 10 should be viewed as the result of a sensitivity study. To address reviewers 2 and 3 comments about this we have conducted additional numerical experiments for which it was assumed that the length of the lead decreases when the pressure at the boundaries increases (see the new Fig.11).

(1) Also the authors state that care has been made to avoid all deformation within the model grid, what limitations does this put on the study?

(2) In the initially submitted manuscript the following text was included:

(3) "Also, in reality, sea ice convergence can cause ridging which can locally increase the yield strength of the ice. This strain hardening process was not considered in our numerical experiments; the maximum possible pressure in the domain is equal to $P^* h_l$."

(2) We have added a few additional sentences about the limitations of our numerical setup in the conclusion.

(1) The authors mention that there is vast literature on ships navigating ice, does any of this describe the situation being simulated?

(2) In the revised manucript, we have improved the text presenting these other studies (see the introduction). We have also described better how our study is different than what was done by others. We have added the following sentences in the revised manuscript:

(3) "In contrast with studies mentioned in the last paragraph, we focus on ship besetting, rather than on a ship progressing in an ice covered region. We also study the downscaling of sea ice pressure from the km scale to scales relevant for navigation activities (tens of m)."

(3) "Idealized sea ice modeling studies with a continuum based approach have been conducted by specifying strain rates at the boundaries (e.g. Kubat et al. (2010); Ringeisen et al. (2019)) or by specifying wind patterns (e.g. Hutchings et al. (2005); Heorton et al. (2018)). However, to our knowledge, it is the first time that internal stresses are specified at the boundaries."

(1) In particular it would be helpful to discuss whether the modelled setup of a lead created by a ship within ice under uniform pressure, results in the lead remaining open and thus increased lead tip pressure existing as modelled here, is a likely and realistic scenario. I am not convinced that ice under uniform external pressure, when passed through by a ship will not result in lead closure, thus allowing the modelled setup to be encountered.

(2) We agree. Please see our other comment above about the new experiments and figure.

(1) I find the results and numerical stability sections confusingly arranged. Further sub sectioning to break apart the various studies in the results will help. Collecting together all the cases where the model resolution was varied would be beneficial. After I had worked out what experiments had been performed and how they related to each I found them clear and well documented.

(2) We think the stability analysis should stay in an appendix as it is not essential for understanding this study. Following the reviewer's advice, we have added these two subsections in the result section:

(3) "Idealized sea ice experiments"

(3) "Experiments with an idealized ship"

(1) Title I find that the title is not an accurate description of the paper content. The paper is focusing particularly on recreating the internal ice stresses at lead tips during constant ice compression for the case of ice stresses being low enough to not cause the closing of the lead. The paper content doesn't give a general method of downscaling as all the model setup is directly for the model case presented. The paper title should reflect this.

(2) We think that the word "Toward" in the title indicates that we do not provide a complete method for downscaling the sea ice pressure. We have nevertheless changed the title so that it better reflects the fact that the goal of the method would be for navigation purposes. The new title is:

(3) "Toward a method for downscaling sea ice pressure for navigation purposes."

(1) Abstract L6 Can you explain what form of numerical experiments you perform in this study within the abstract? A little extra depth on the nature of the methods used will be helpful here.

(2) We have modified one sentence in the abstract in the revised manuscript. The sentence is:

(3) "In this paper, the downscaling of sea ice pressure from the km-scale to scales relevant for ships is investigated by conducting high resolution idealized numerical experiments with a viscous-plastic sea ice model"

(1) L10 The information within the parenthesis does'nt correspond well to the

rest of the sentence. Do you mean that your study reveals that that the lead length is particularly important?

(2) The end of the abstract has been modified in the revised manuscript.

(1) L13 I will be helpful here to clearly indicate that ice pressure is a horizontal 2d force.

(2) We have added the following sentence in section 2:

(3) "As the stresses are vertically integrated, the stresses and stress invariants are 2D fields with units of $\mathbf{Nm^{-1}}$"

(1) L15 can you define "ship besetting"

(2) We don't think this needs to be defined.

(1) L16 predict the pressure field from what? using a force balance of applied wind, ocean stresses and sea ice drift.

(2) The following sentence is in the revised manuscript:

(3) "By solving equations for the momentum balance and for the ice thickness distribution, sea ice models are able to predict the evolution of the pressure field.

(1) L50 It might be helpful to include a brief introduction of previous square box ice modelling studies. VP simulations

More VP
Hutchings, J.K. et al. 2005. Modeling Linear Kinematic Features in Sea Ice. Monthly Weather Review. 133, 12 (Dec. 2005), 3481 - 3497.

Using CICE
Heorton, H.D.B.S. et al. 2018. Stress and deformation characteristics of sea ice in a high-resolution, anisotropic sea ice model. Phil. Trans. R. Soc. A. 376, 2129 (Sep. 2018), 20170349.

Discrete element modelling
Wilchinsky, A.V. et al. 2010. Effect of shear rupture on aggregate scale formation in sea ice. Journal of Geophysical Research. 115, C10 (Oct. 2010). DOI:https://doi.org/10.1029/2009JC006043.

(2) We agree. We have added in the introduction the following text with some references:

(3) "Idealized sea ice modeling studies have been conducted by specifying strain rates at the boundaries (e.g. Kubat et al. (2010); Ringeisen et al.(2019)) or by specifying wind patterns (e.g. Hutchings et al. (2005); Heorton et al. (2018)). However, to our knowledge, it is the first time that internal stresses are specified at the boundaries."

(1) L114 equation 9. All previous equations are well described, Can you explain the physical reasoning for the replacement closure as well?

(2) We have added the following sentence:

(3) "The replacement pressure is commonly used in sea ice models to prevent unrealistic deformations of the sea ice cover when there is no external forcing."

(1) L149 An overview explanation here will make the following equations much easier to follow. From what I can tell you impose the total normal and shear stresses. The equations that follow enable you to give the components of the gradient of the internal stress tensor. Is this correct?

(2) We have added the following text in section 5:

(3) "In all the experiments, normal and shear stresses are applied at the four boundaries of the 5×5 km domain. For a given set of sea ice conditions, the steady-state solution of equation (10) is obtained. This provides us with the velocity field defined on the Arakawa C-grid. As the stresses and invariants are function of the sea ice conditions and velocity (see equations(2-9)), static 2D fields of the internal stresses and invariants are easily obtained."

(1) L159 does this mean that v(1m) will be solved for in the model? Can you list the components that need to be imposed for this side of the grid structure and those which will be left free?

(2) We have added the following text in section 4:

(3) "Even though $u_{(1m)}$ is located at the boundary, it is solved along with $v_{(1m)}$ and all the other velocity components in the domain by the nonlinear solver."

(1) L165 what happens to this simulation when the normal stress on the east and west side are not equal? I assume that there will be a large E-W ice drift which i understand is best avoided for your study. This information will be very helpful for those who wish to recreate your model setup.

(2) The simulation blows up when the normal stress on the east and west sides are not equal. The reader is referred to the appendix for further explanations.

(1) L168 This information doesn't require its own section, though including it is very useful. Perhaps put it with the coarse grain results, or in the previous or following section. Actually if all the methods are placed in a "methods" section and subsections are used the paper format will be easier to navigate.

(2) We agree. As suggested, we have moved the figure to the result section.

(1) L175 so you have two masks - one defines the ship internal, one defines the ship contour. On which contour iare the ice force balance equations solved? This section defines the technical boundary conditions of the mask, but a descriptive overview of what is done where on which mask will aid the readability of the technical description.

(2) We have decided to simplify the way the digitized ship is defined. The ship is defined by land cells. The boundary conditions are no slip and no outflow. This is explained in the description of the experimental setup (section 3 in the revised manuscript). The masks Mi and Mc are not required anymore. Note that this leads to results qualitatively the same and allows us to draw the same conclusion.

(1) L181 does the ship ice strength imply that this ship is deformable? Was this done for realism or to allow the model to run effectively?

(2) See our response above.

(1) L183 Is the ships resistance to shear representing the shear strength at the ice/ship hull interface (so a form of friction between ice and steel) or the resistance the ship itself has to shearing? I guess the former as it seems as if the ship itself can not deform as it is fixed to the grid.

(2) See our response above.

(1) L189 ah you 've mentioned the ice sliding around the ship. Do you apply different shear condition for each mask?

(2) See our response above.

Section 7 (1) Can you include some basic information about the model setup either here or back in section 3? What model simulations are you seeking? It seems that you are looking for static solutions, invariant in time, or a snap shot of ice stress, is this the case? What are you hoping to show us with these validations? You are comparing to idealised numbers of ice pressure. Do these validations show that the numerical model generates the correct pressures for a static field? For the lead cases presented here i was expecting to see the closing of the lead, though this makes little sense if the simulations just show the immediate pressure field of ice with a lead present.

(2) See our other responses above. We think we have improved the text in the introduction and in sections 3-6 of the revised manuscript. About the validation, the following sentence of the revised manuscript helps to understand how the pressure is simulated:

(3) "For a given set of sea ice conditions, the steady-state solution of equation (10) is obtained. This provides us with the velocity field defined on the Arakawa C-grid. As the stresses and invariants are function of the sea ice conditions and velocity (see equations (2-9)), static 2D fields of the internal stresses and invariants are easily obtained."

(1) From reading ahead to the results it appear you are particularly interested in the increased stresses in the ice at the end of a lead, which a location where a ship is likely to be present. Informing the reader of this before the validation section will show why you are checking the pressure states to show that these regions are correctly simulated.

(2) We have reworked the introduction. We think that the following sentences inform the reader about the ship experiments:

(3) "...we focus on ship besetting, rather than on a ship progressing in an ice covered region. We also study the downscaling of sea ice

pressure from the km scale to scales relevant for navigation activities (tens of m).”

(3) “For our numerical experiments, we use a continuum based viscous-plastic sea ice model. In a first set of simulations, we study how the small-scale pressure depends on the stresses applied at the boundaries, on the ice conditions and on the rheology parameters. The second part of the results is dedicated to shipping applications; we investigate the small-scale pressure field in the vicinity of an idealized ship beset in heavy ice conditions and under compressive stresses.”

(1) L207 how is it obtained from the model?

(2) See our other responses above. We think that the manuscript is clearer.

(1) L222 what conclusions will you be seeking in the results section? The validations show that your model is good for the stress states you hope to test, but to fully show this you need to state what these stress states are and why the model and its setup work for them.

(2) See our other responses above. We think we have addressed these points in the revised manuscript.

(1) L350 my understanding is that the model gives the solution of a single "snapshot" of ice stress. The acceleration argument then surely does not matter?

(2) We understand that this was confusing. We have modified the text and have redone the simulations in order to find the steady-state solution of $\rho h \partial u/\partial t = \nabla \cdot \sigma$. This is equivalent as solving for $\nabla \cdot \sigma = 0$ (both approaches give the same answer). This is now consistent with the stability analysis described in the appendix.

Jean-François Lemieux

Toward a method for downscaling sea ice pressure for navigation purposes

Jean-François Lemieux[1], Bruno Tremblay[2], and Mathieu Plante[2]

[1]Recherche en Prévision Numérique Environnementale/Environnement et Changement Climatique Canada, 2121 route Transcanadienne, Dorval, Qc, Canada.
[2]Department of Atmospheric and Oceanic Sciences, McGill University, Montréal, Qc, Canada.

Correspondence: Jean-François Lemieux (jean-francois.lemieux@canada.ca)

Abstract. Sea ice pressure poses great risk for navigation; it can lead to ship besetting and damages. Contemporary large-scale sea ice forecasting systems can predict the evolution of sea ice pressure. There is, however, a mismatch between the spatial resolution of these systems (a few km) and the typical dimensions of ships (a few tens of m) navigating in ice-covered regions. In this paper, ~~we investigate~~ the downscaling of sea ice pressure from the km-scale to scales relevant for ships is investigated by conducting high resolution idealized numerical experiments with a viscous-plastic sea ice model. Results show that sub-grid scale pressure values can be significantly larger than the large-scale pressure (up to $\sim 4\times$ larger in our numerical experiments). High pressure at the sub-grid scale is associated with the presence of defects (e.g. a lead). Numerical experiments show ~~that a ship creates its own high stress concentration by forming a lead in its wake while navigating~~significant stress concentration on both sides, especially at the back, of a ship beset in sea ice. The magnitude of the stress concentration increases with the length of the lead (or channel) behind the ship and decreases as sea ice consolidates either by thermodynamical growth or mechanical closing. These results also highlight the difficulty of forecasting, for navigation applications, the small-scale distribution of pressure and especially the largest values ~~. Indeed, this distribution strongly depends on variables that are not well constrained: the rheology parameters and the small-scale structure of sea ice thickness (more importantly~~ as the important parameters (i.e., the length of the lead behind the ship ~~)~~and the thickness of the refrozen ice) are not well constrained.

1 Introduction

With the growing shipping activities in the Arctic and surrounding seas, there is a need for user relevant sea ice forecasts and products at multiple time and spatial scales. An important forecast field for navigation is the internal sea ice pressure (simply referred to as pressure for the rest of this paper). In compact ice conditions, high pressure events can complicate navigation activities and even pose great risk for ship besetting.

~~With the use of constitutive equations (or rheology)~~By solving equations for the momentum balance and for the ice thickness distribution, sea ice models are able to predict the evolution of the pressure field. However, even for high resolution operational forecasting systems with spatial resolutions of a few km (e.g. Dupont et al. (2015); Hebert et al. (2015)), there is a clear mismatch in the spatial scales considered. Indeed, the forecast pressure from the model, which represents the average pressure for a

grid cell of a few km wide, is not necessarily relevant for a much smaller ship; there are larger pressure values than the average pressure provided by the sea ice forecasting system (Kubat et al., 2010; Leisti et al., 2011; Kubat et al., 2012). Figure 1 shows an example of a pressure forecast from a large-scale forecasting system. The Canadian Arctic Prediction System (CAPS) is a fully-coupled atmosphere-sea ice-ocean system developed and maintained by the Canadian Centre for Meteorological and Environmental Prediction. Its domain covers the Arctic Ocean, the North Atlantic and the North Pacific. The spatial resolution of the atmospheric model is ∼3 km while the spatial resolution in this region for the sea ice and ocean models is ∼4.5 km. Looking at a specific region, that is north of Svalbard (panel b), it can be observed that the surface winds push the ice toward the coast and create large pressure.

~~Kubat et al. (2010) conducted idealized numerical simulations of a ship transiting through a loose sea ice cover. They showed that the pressure on the hull of the ship can be two orders of magnitude larger than the large-scale pressure. Through a parameter sensitivity study, they also demonstrated that ship velocity has the most pronounced impact on the total ice force applied on the ship.~~

Some researchers have ~~also~~ done case studies of compressive or besetting events using large-scale sea ice forecasting systems (e.g. Kubat et al. (2012); Leisti et al. (2011); Kubat et al. (2013)). These besetting events are all associated with heavy ice conditions. The investigations of Kubat et al. show the importance of the coast on pressure conditions; the sea ice pressure often increases toward the coast.

Mussells et al. (2017) used ship logs and satellite imagery to relate besetting events and density of sea ice ridges. They indeed found that the ship was often beset in areas and times of the year with high ridge densities. Probabilistic models for ship performance in sea ice and likelihood of besetting events have also been developed (e.g. Montewka et al. (2015); Turnbull et al. (2019)). Turnbull et al. (2019) argue that the primary cause of the besetting events they studied were the relatively large ice floes encountered by the vessel.

There is also a vast literature on the performance of ships navigating in ice infested waters and on the estimation of ice resistance, that is the longitudinal forces applied on the ship by the ice ~~.~~(e.g., Lindqvist (1989); Su et al. (2010); Jeong et al. (2017)). These calculations are important for ship design and for operational considerations. Lindqvist (1989) introduced a simple empirical formulation to calculate ice resistance based on ship's characteristics and ice ~~conditions. Numerical models of ships navigating in level ice that consider~~ physical parameters. When sea ice pressure is not considered, the resistance encountered by a ship only depends on processes such as ~~crushing and bending failure have also been proposed (e. g., Su et al. (2010); Lubbad and Loset (2011); Jeong et al. (2017))~~on crushing, breaking and displacement of ice floes by the ship's hull. Based on laboratory experiments in ice tanks, Kulaots et al. (2013) extended this empirical approach by also considering the effect of compression on the performance of ships navigating in ice infested waters. There are also some numerical studies of ice loads on ships ~~by representing the sea ice as~~ transiting in ice infested waters where sea ice is represented using discrete

elements (i.e., the floes, Metrikin and Løset (2013); Daley et al. (2014)) ~~.~~or as a continuum (e.g., Kubat et al. (2010)).

~~In this paper, we use a continuum based viscous-plastic sea ice model to investigate~~

In contrast with studies mentioned in the last paragraph, we focus on ship besetting, rather than on a ship progressing in an ice covered region. We also study the downscaling of sea ice pressure from the km scale to scales relevant for navigation activities (tens of m). Note that this was briefly investigated by Kubat et al. (2010) for a ship transiting through a loose sea ice cover. Kubat et al. (2010) showed that the pressure on the hull of the ship can be two orders of magnitude larger than the large-scale pressure. For our numerical experiments, we use a continuum based viscous-plastic sea ice model. In a first set of simulations, we study how the small-scale pressure depends on the stresses applied at the boundaries, on the ice conditions and on the rheology parameters. The second part of the results is dedicated to shipping applications; we investigate the small-scale pressure field in the vicinity of an idealized ship beset in heavy ice conditions and under compressive stresses. Idealized sea ice modeling studies with a continuum based approach have been conducted by specifying strain rates at the boundaries (e.g. Kubat et al. (2010); Ringeisen et al. (2019)) or by specifying wind patterns (e.g. Hutchings et al. (2005); Heorton et al. (2018)). However, to our knowledge, it is the first time that internal stresses are specified at the boundaries.

This paper is structured as follow. In section 2, the sea ice momentum equation and the viscous-plastic rheology are described. The sea ice model used for the numerical experiments is presented in section 3. The approach for prescribing sea ice stresses at the boundaries is presented in section 4. ~~A coarse-graining procedure to define sea ice conditions is described in section ??. A digitized ship is used for some numerical experiments. The implementation of this digitized ship is presented in section ??. The~~ The validation of our experimental setup is done in section 5. The main results are given in section 6. Finally, concluding remarks are provided in section 7.

2 Sea ice momentum equation and rheology

Large-scale sea ice forecasting system solves the sea ice momentum given by

$$\rho h \frac{D\mathbf{u}}{Dt} = -\rho h f \hat{\mathbf{z}} \times \mathbf{u} + \tau_a - \tau_w + \nabla \cdot \sigma - \rho h g \nabla H_d, \tag{1}$$

where ρ is the density of the ice, h is the ice volume per unit area (~~or the mean thickness and just~~ sometimes referred to as ~~thickness in this paper~~the mean thickness), $\frac{D}{Dt}$ is the total derivative, f the Coriolis parameter, $\mathbf{u} = u\hat{\mathbf{x}} + v\hat{\mathbf{y}}$ the horizontal sea ice velocity vector, $\hat{\mathbf{x}}$, $\hat{\mathbf{y}}$ and $\hat{\mathbf{z}}$ are unit vectors aligned with the x, y and z axis of our Cartesian coordinates, τ_a is the wind stress, τ_w the water stress, σ the internal ice stress tensor with components σ_{ij} acting in the jth direction on a plane perpendicular to the ith direction, g the gravitational acceleration and H_d the sea surface height. This two-dimensional formulation, which is obtained by integrating along the vertical, is justified when the ratio between the horizontal and vertical scales of the problem

is large (i.e., a ratio of at least 1:10, Coon et al. (1974)).

The sea ice pressure is by definition the average of the normal stresses, that is

$$p = -(\sigma_{11} + \sigma_{22})/2, \tag{2}$$

with a negative sign because, by convention, stresses in compression are negative. The ~~sea ice~~ pressure is the first stress invariant (i.e., it does not vary with the choice of the coordinate system). The second stress invariant (q), that is the maximum shear stress at a point, is defined by

$$q = \sqrt{\sigma_{12}^2 + \left[\frac{(\sigma_{11} - \sigma_{22})}{2}\right]^2}. \tag{3}$$

As the stresses are vertically integrated, the stresses and stress invariants are 2D fields with units of Nm^{-1}. Because the sea ice stresses are written as a function of the sea ice velocity (see details below), one also obtains the ~~sea ice~~ pressure p and the maximum shear stress q when solving the momentum equation for $\mathbf{u}$. Hence, by solving the momentum equation for the large-scale sea ice model, the pressure at every grid point is obtained (we refer to this pressure field as the large-scale pressure).

Here, we consider a small area of sea ice (the size of a grid cell) to be under compressive stresses. The idea is to apply the large-scale pressure at the boundaries of this small area and to simulate the sub-grid scale sea ice pressure (referred to as the small-scale pressure). We assume here that the ice is not moving nor deforming (e.g. it is being held against a coast). To further simplify the problem, the wind stress, the water stress, the advection of momentum and the sea surface tilt term are neglected. ~~This means that we~~ We wish to find~~the solution of $\nabla \cdot \sigma = 0$~~, inside this small domain, the steady-state solution of $\rho h \partial \mathbf{u}/\partial t = \nabla \cdot \sigma$ which is equivalent as finding the solution of $\nabla \cdot \sigma = 0$. The stresses are modeled according to the viscous-plastic rheology with an elliptical yield curve (Hibler, 1979). With this rheology, the relation between the stresses and the strain rates can be written as

$$\sigma_{ij} = 2\eta\dot{\epsilon}_{ij} + [\zeta - \eta]\dot{\epsilon}_{kk}\delta_{ij} - P\delta_{ij}/2, \quad i,j = 1,2, \tag{4}$$

where δ_{ij} is the Kronecker delta, $\dot{\epsilon}_{ij}$ are the strain rates defined by $\dot{\epsilon}_{11} = \frac{\partial u}{\partial x}$, $\dot{\epsilon}_{22} = \frac{\partial v}{\partial y}$ and $\dot{\epsilon}_{12} = \frac{1}{2}(\frac{\partial u}{\partial y} + \frac{\partial v}{\partial x})$, $\dot{\epsilon}_{kk} = \dot{\epsilon}_{11} + \dot{\epsilon}_{22}$, ζ is the bulk viscosity, η is the shear viscosity and P is a term which is a function of the ice strength.

The bulk and shear viscosities are respectively

$$\zeta = \frac{P_p}{2\triangle}, \tag{5}$$

$$\eta = \zeta e^{-2}, \tag{6}$$

where P_p is the ice strength, $\triangle = \left[(\dot{\epsilon}_{11}^2 + \dot{\epsilon}_{22}^2)(1+e^{-2}) + 4e^{-2}\dot{\epsilon}_{12}^2 + 2\dot{\epsilon}_{11}\dot{\epsilon}_{22}(1-e^{-2})\right]^{\frac{1}{2}}$, and e is the aspect ratio of the ellipse, i.e. the ratio of the long and short axes of the elliptical yield curve.

Following Hibler (1979), the ice strength P_p is parameterized as

$$P_p = P^* h \exp[-C(1-A)], \tag{7}$$

where P^* is the ice strength parameter, A is the sea ice concentration and C is the ice concentration parameter, an empirical constant set to 20 (Hibler, 1979) such that the ice strength decreases quickly with the ice concentration. Unless otherwise stated, the rheology parameters P^* and e are respectively set to 27.5 kNm^{-2} and 2.

When $\triangle$ tends toward zero, equations (5) and (6) become singular. To avoid this problem, ζ is capped ~~using an hyperbolic tangent (Lemieux and Tremblay, 2009)~~ following the approach of Hibler (1979). It is expressed as

~~$\zeta = \zeta_{max} \tanh(\frac{P_p}{2\triangle\zeta_{max}}).$~~

$$\zeta = \frac{P_p}{2\Delta^*}, \tag{8}$$

~~As in equation (6), $\eta = \zeta e^{-2}$. The coefficient ζ_{max} is set to the value proposed by Hibler (1979): $2.5 \times 10^8 P_p$ (this is equivalent to limiting $\triangle$ to a minimum value of 2×10^{-9}~~where $\Delta^* = \max(\Delta, \Delta_{min})$ with $\Delta_{min} = 2 \times 10^{-9}$ s^{-1}~~).~~.

We use a replacement ~~closure~~ method similar to the one presented in Kreyscher et al. (2000). The P term in equation (4) is given by

$$P = 2\zeta\triangle. \tag{9}$$

The replacement method is commonly used in sea ice models to prevent unrealistic deformations of the sea ice cover when there is no external forcing.

3 Experimental setup

The McGill sea ice model is used for the numerical experiments. We use revision 333 with some modifications, described below, for specifying stresses at the boundaries.

Considering a domain of a few km by a few km wide (representing a grid cell of a large-scale sea ice forecasting system), the idea is to use the model at very high resolution for studying the distribution of pressure inside that domain. To do so, the model was modified so that internal stresses can be specified at the boundaries (instead of the usual Dirichlet condition (i.e. $\mathbf{u} = 0$) at land-ocean boundaries and the Neumann condition at open boundaries with gradients of velocity equal to zero). These stresses at the boundaries represent the integrated effect of the wind and ocean-ice stresses (like one would get from a large-scale model). The next section gives more details about the implementation of the stress boundary conditions.

For the experiments, the domain is a square of dimensions 5.12 km by 5.12 km. It is subdivided in small squared grid cells of dimensions Δx by Δx with Δx taking one of the following values depending on the experiment: 10 m, 20 m, 40 m, 80 m, 160 m, 320 m, 640 m or 1280 m. The size of the domain was chosen because it is close to the average size of CAPS sea ice grid cells and because 5120 m divided by the Δx listed above gives an integer number ~~(n)~~ of small grid cells. For simplicity, we refer to this domain as our 5×5 km domain.

The momentum equation $\rho h \partial \mathbf{u}/\partial t = \nabla \cdot \sigma$ is solved at time levels Δt, $2\Delta t$, $3\Delta t$, ... where Δt is the time step. We introduce the index $n = 1, 2, 3, \ldots$ which refers to these time levels. Using a backward Euler approach for the time discretization, the momentum equation is written as

$$\rho h \frac{u^n - u^{n-1}}{\Delta t} = \nabla \cdot \sigma^{\mathbf{n}} \tag{10}$$

The spatial discretization of ~~$\nabla \cdot \sigma = 0$~~ equation (10) on the McGill model Arakawa C-grid leads to a system of nonlinear equations that is solved using a Jacobian free Newton Krylov (JFNK) solver ~~with~~ (the most recent version is described in Lemieux et al. (2014)~~. The~~). The ice starts from rest. The time step is 30 min. At each time level, the nonlinear convergence criterion is reached when the Euclidean norm of the residual has been reduced by a factor of ~~10^6.~~ 10. The maximum number of nonlinear iterations is set to 500. The steady-state solution is assumed when the maximum velocity difference between two time levels is lower than 10^{-9} m s^{-1}. As the ice is assumed to be held against the coast, the simulated velocities are very small (i.e., most of the ice cover is in the viscous regime). Our numerical simulations therefore provide 2D static fields of the internal stresses inside this small domain. Thermodynamic processes and advection of h and A are neglected for all the numerical experiments described in this paper.

For some of the numerical experiments, a digitized ship is placed inside the domain. The digitized ship is simply defined as a rigid body by using land cells. The boundary conditions on the contour of the ship are therefore no outflow and no slip (i.e., $u = 0$) which is the usual Dirichlet approach for land cells. This allows us to investigate the distribution of small-scale pressure around this idealized ship.

4 Boundary conditions for the small domain

The boundary conditions are imposed the same way on the four sides of the small domain. Hence, to shorten the paper, only the treatment on the west side of the domain is explained here. The McGill model uses an Arakawa C-grid; the center of the cell is the point for tracers (e.g. h and A) while the velocity components are positioned on the left side (for u) and lower side (for v). To avoid confusion with the indices i and j for the stresses σ_{ij} and the strain rates $\dot{\epsilon}_{ij}$, the indices l and m are respectively used to identify the grid cells along the x and y axes. The cell at the southwesternmost location of the domain has indices l =1 and m =1. Figure 2 shows one of the grid cell on the first column of the domain (on the west side). The left side of the grid cell is on the west boundary of the domain. The sides of the domain are referred to as west (W), east (E), south (S) and north (N).

On the west side of the domain, a normal stress (σ^W) and a shear stress (τ^W) are applied. The momentum balance for the u component is comprised of the terms $\partial\sigma_{11}/\partial x$ and $\partial\sigma_{12}/\partial y$. Inside the domain, these terms are approximated by second-order centered differences. At the boundaries, however, a one-sided first-order approximation is employed for $\partial\sigma_{11}/\partial x$. Hence, $\partial\sigma_{11}/\partial x$ at the u location $u(l,m) = u_{(lm)}$ with l =1 is approximated as

$$\frac{\partial\sigma_{11}}{\partial x} \sim \frac{\sigma_{11(1m)} - \sigma^W_{(m)}}{\Delta x/2}, \tag{11}$$

where $\sigma_{11(1m)} = [\zeta_{(1m)} + \eta_{(1m)}][u_{(2m)} - u_{(1m)}]\Delta x^{-1} + [\zeta_{(1m)} - \eta_{(1m)}][v_{(1m+1)} - v_{(1m)}]\Delta y^{-1} - P_{(1m)}/2$ is evaluated at the t point.

On the other hand, the term $\partial\sigma_{12}/\partial y$ only depends on the boundary conditions, that is

$$\frac{\partial\sigma_{12}}{\partial y} \sim \frac{\tau^W_{(m+1)} - \tau^W_{(m)}}{\Delta y}, \tag{12}$$

~~This means that even though $u_{(1m)}$ is located at the boundary, it is also solved by the nonlinear solver.~~

For the v component $v_{(1m)}$ (which is at a distance of $\Delta x/2$ from the boundary), there is no special treatment for $\partial\sigma_{22}/\partial y$. However, the second-order treatment of the term $\partial\sigma_{12}/\partial x$ follows

$$\frac{\partial\sigma_{12}}{\partial x} \sim \frac{\sigma_{12(2m)} - \tau^W_{(m)}}{\Delta x}, \tag{13}$$

where $\sigma_{12(2m)} = \eta_{(2m)}[u_{(2m)} - u_{(2m-1)}]\Delta y^{-1} + \eta_{(2m)}[v_{(2m)} - v_{(1m)}]\Delta x^{-1}$ is evaluated at the n point.

Even though $u_{(1m)}$ is located at the boundary, it is solved along with $v_{(1m)}$ and all the other velocity components in the domain by the nonlinear solver.

In our simulations, $\sigma^W_{(m)} = \sigma^W$ and $\tau^W_{(m)} = \tau^W$, i.e., they do not vary with m along the boundary (same idea for the other sides of the domain). Furthermore, for numerical stability (see appendix A), the normal stress on the east side (σ^E) has to be equal to σ^W. Similarly, $\sigma^S = \sigma^N$ and $\tau^W = \tau^E = \tau^S = \tau^N$.

5 ~~Coarse-graining procedure~~

~~For some of the results, a coarse-graining procedure is used to obtain low resolutions ice conditions from h and A fields defined at high resolution. This procedure is explained in Fig. 7.~~

~~Schematic of the coarse-graining procedure. The thickness field is defined at 10 m resolution (blue cells on the left). The thickness field at 20 m resolution is obtained by averaging the h values of the four 10 m cells contained in the 20 m one (purple cell). This procedure is repeated for the other lower resolutions. The same method is applied for the concentration A. The indices l, m are for the 10 m grid while the indices l^*, m^* are for the 20 m grid.~~

5 ~~Idealized ship~~

~~We have also coded in the model an idealized representation of a ship beset in heavy ice conditions. This allows us to investigate the distribution of small-scale pressure around this idealized ship. Two masks are defined: one mask that represents the inside (i) of the ship at the tracer points (M_i) and one mask M_c that defines the contour (c) of the ship (defined at the n point as shown in Fig. 2). The mask M_i is zero everywhere except at tracer points that define the shape of the ship (i.e., $M_i = 1$). The mask M_c is constructed from M_i; M_c is equal to 1 if the sum of the four neighboring M_i is either 1, 2 or 3.~~

~~The idea is to embed the idealized ship in the sea ice model by specifying special mechanical characteristics at the $M_i = 1$ points and on the contour of the ship (i.e., where $M_c = 1$). First, the strong resistance of the ship in compression is represented by setting the ice strength to βP^* where $M_i = 1$ (this is equivalent to assuming that the ship is sea ice with a thickness of β m). For most of the experiments , β is set to 10.0. This implies that the interior (structure) of the ship also has strong resistance to shear as the ellipse aspect ratio is also set to 2 (i. e., $e_i = e = 2$ where $M_i = 1$). The maximum shear strength is in this case $0.25\beta P^*$.~~

~~The mechanical characteristics of the contour are associated with mechanical interactions between the sea ice and the ship. The model requires the calculation of the η at the n points. For the calculation of the η on the contour of the ship, P_p is assumed to be equal to the ice strength of the level ice (i.e., $P_p = h_l P^*$ which is the mechanical strength of the weakest of the~~

two materials) . Moreover, it is assumed that the ice can slide relatively easily on the side of the ship. To represent this, the shear strength on the ship contour (i. e., where M_c=1) is set to a smaller value than the one for sea ice. This is done by specifying a larger ellipse ratio on the contour (e_c) than the value specified for sea ice (e) and inside the ship (e_i). Hence, $e_c = \kappa e$ with $\kappa >$ 1 and e =2 for the experiments with the ship. For most of these experiments, κ is set to 5.0.

5 Model validation

The McGill model has, over the years, been extensively tested (e.g. Lemieux et al. (2014); Bouchat and Tremblay (2017); Williams and Tre). A few simple experiments were conducted in order to validate the implementation of the new stress boundary conditions.

The McGill model has, over the years, been extensively tested (e.g. Lemieux et al. (2014); Bouchat and Tremblay (2017); Williams and T). A few simple experiments were conducted in order to validate the implementation of the new stress boundary conditions.
In all the experiments, normal and shear stresses are applied at the four boundaries of the 5×5 km domain. For a given set of sea ice conditions, the steady-state solution of equation (10) is obtained. This provides us with the velocity field defined on the Arakawa C-grid. As the stresses and invariants are function of the sea ice conditions and velocity (see equations (2-9)), static 2D fields of the internal stresses and invariants are easily obtained.

Compared to realistic pan-Arctic simulations, the simplicity of the problem allows one to obtain analytical solutions for specific cases. In a first validating experiment, the thickness (h) and concentration (A) fields are respectively set to ~~1~~ 2 m and 1 everywhere on the domain. By specifying $\sigma^W = \sigma^E = \sigma^S = \sigma^N$ = -10 kNm^{-1} (i.e., p =10 kNm^{-1}) and $\tau^W = \tau^E = \tau^S = \tau^N$ = 0 kNm^{-1}, at the boundaries, the shear stress should be zero everywhere inside the domain while the pressure field should be constant and equal to 10 kNm^{-1}. This is indeed what is obtained from the numerical experiment (not shown). With p =10 kNm^{-1}, a ~~1~~ 2 m ice cover is able to resist this compressive stress, that is the ice should be in the viscous regime. Using the definition of the stresses from equation (4), we obtain $p = P/2 - \zeta\dot{\epsilon}_I$, where $\dot{\epsilon}_I = \dot{\epsilon}_{11} + \dot{\epsilon}_{22}$ is the divergence. ~~To simplify the problem here, the replacement pressure is not used (i.e., $P = P_p$) and the simple capping approach of Hibler (1979) for ζ is employed instead of the capping given by equation **??**. With these assumptions, the analytical solution is $\dot{\epsilon}_I = 5.18 \times 10^{-10}$~~ It is easy to demonstrate that the analytical solution for the divergence is $\dot{\epsilon}_I = -p\Delta_{min}/P_p = -3.63 \times 10^{-10}$ s^{-1}~~, which~~ . This is exactly what is obtained with the model (not shown).

We also verify that we obtain the same results when a lead is present within the physical domain for different spatial resolution (Δx). For example, Fig. 3 shows the pressure field for a 1 km long, 40 m wide lead resolved with a Δx of 10 m (a) and for the same lead resolved with Δx =20 m (b). The thickness of the level ice (h_l) around the lead is 2 m.. The maximum pressure at 10 m resolution is ~~31.42~~ 35.79 kNm^{-1} while the maximum pressure at 20 m is ~~29.09~~ 33.15 kNm^{-1}. ~~The~~ From these simulated 2D pressure fields, probability density functions (PDF~~,~~) are calculated using bins of 0.25 kNm^{-1}. They are shown

in Fig. 3c ~~) also demonstrate~~ which further demonstrates that the simulated fields are very similar at 10 and 20 m resolutions.

The effect of the same lead but oriented differently in the domain was also tested. The PDF of the pressure field is exactly the same whether the lead is oriented horizontally (west-east) or vertically (south-north, not shown). The spatial distribution of pressure is qualitatively the same when orienting the lead diagonally. The PDF of pressure for this diagonal lead is similar to the PDF of the vertical and horizontal ones although we find that the maximum pressure is usually a bit smaller (not shown). This is likely a consequence of the spatial discretization of a finite width lead on a cartesian grid.

In a last set of experiments for the validation, we also checked that the presence of relatively nearby boundaries do not affect our conclusions. In the first experiment, ~~a horizontal 1.5~~ with Δx =20 m, a horizontal 1 km long and 20 m wide lead was positioned in the center of the 5.12 km by 5.12 km domain. In a second experiment, again with Δx =20 m, the same lead was positioned in a domain twice this size, that is the boundaries are much further from the lead in the second experiment. For both experiments, h_l is again equal to 2 m. The pressure fields around the lead are very similar (not shown) in the two experiments with maximum pressures in the domain equal respectively to ~~22.77~~ 36.22 kNm^{-1} and ~~23.02~~ 36.36 kNm^{-1} (a difference of $\sim$ ~~1~~0.4%). To avoid these boundary effects, we will tend to position the important features in the center of the domain for the numerical experiments. For a numerical experiment to be valid, we require that the simulated pressure in the first grid cells around the domain has to be within 10% of the pressure value specified at the boundaries.

6 Results

To limit the number of parameters than can be varied in the numerical experiments, the thickness of the level ice h_l is always set to 2 m. Furthermore, for all the experiments, except the ones for the last figure, the normal stresses at the boundaries are always equal to -10 kNm^{-1} while the shear stresses are set to zero. In other words, $\sigma^W = \sigma^E = \sigma^S = \sigma^N = -10$ kNm^{-1} and $\tau^W = \tau^E = \tau^S = \tau^N = 0$ kNm^{-1}.

6.1 Idealized sea ice experiments

In a first set of experiments, we conduct idealized experiments to investigate the impact of sea ice features (leads, ridges, etc.) on the small-scale pressure field and especially on the maximum pressure. These experiments will give us insights and guide us for the second series of experiments with the idealized ship (see subsection 6.2). Fig. 4a shows the pressure field for a uniform sea ice cover with $h_l = 2$ m except the presence of a ~~long~~ 1 km ~~lead. We have introduced h_l with the subscript 'l' referring to as 'level' ice.~~ long and 10 m wide lead. Large pressure are observed at the tips of the lead. In a second experiment, the same thickness sea ice conditions are used except that a smaller lead, a refrozen lead (with $h = 0.5$ m) and a thick sea ice ridge (with $h = 5$ m) are also positioned in the 5×5 km domain. The pressure field for this latter experiment is shown in Fig. 4b. Fig. 4c

compares the PDFs of pressure for these two experiments. Looking at the PDFs and comparing Fig. 4a and Fig. 4b, one can notice that the other features are not associated with such high pressure values and that the maximum pressure is associated with the long 1 km lead. To further support this conclusion, note that the maximum pressure in the 5×5 km domain is ~~38.19~~ 42.57 kNm^{-1} in the first experiment while it is ~~38.35~~ 42.59 kNm^{-1} in the second one. In other words, the other features do not change our analysis; what really matters is the longest lead as it is in the vicinity of the longest lead that the largest stress concentration is found.

Our results above suggest that only the longest lead needs to be considered for estimating the largest small-scale pressure. For a given h_l and stresses applied at the boundaries, there is more and more stress concentration when increasing the length of a lead. This is shown in Fig. 5 for three values of the parameter P^*. For short leads, the ice around the lead is able to sustain the stresses (the ice is rigid, that is in the viscous regime). This is why the three curves are very similar in Fig. 5a and Fig. 5b for short leads. However, for longer leads, there is more and more stress concentration. Some points of the ice, close to the tips of the lead, fail (i.e., the state of stress reaches the yield curve).

As the whole yield curve scales with the value of P^*, a larger P^* leads to larger maximum pressure and shear values. When increasing P^*, the maximum shear stress approaches asymptotically the shear strength (dashed lines in panel a, $e^{-1}h_l P^*/2$). This asymptotic behavior is less obvious for the pressure (Fig. 5b) as it is still far from the compressive strength ($h_l P^*$). A similar behavior is observed when varying the ellipse aspect ratio (which modifies the shear strength). A smaller value of e leads to larger pressure values and larger shear stresses values (with a similar asymptotic behavior) for long leads (not shown).

While the average pressure in the domain is the same (10 kNm^{-1}) for all the values of P^*, the maximum pressure is enhanced as P^* increases (as shown in Fig. 5b). Comparing the pressure fields with P^*=27.5 kNm^{-2} and P^*=20 kNm^{-2} (see Fig. 6) for the same lead shows that the pressure fields around the lead are different over hundreds of meters. Moreover, the largest difference in the pressure fields are found at the tips of the lead; the pressure is much larger with P^*=27.5 kNm^{-2} than with P^*=20 kNm^{-2} in the vicinity of the tips.

We also investigate the evolution of the small-scale pressure field as a function of resolution. The h and A fields are defined at 10 m resolution. These fields h and A are respectively set to 2 m and 1.0 everywhere except for a 1 km long, 10 m wide lead in the middle of the domain with $h = 0$ m and $A = 0$. The model is run at resolutions of 10, 20, 40,...1480 m. For these lower resolutions, the h and A fields are obtained through ~~the~~ a coarse-graining procedure (see Fig. 7 for details).

All the values of p and q in the 5×5 km domain are plotted as a function of Δx in Fig. 8a and Fig. 8b. The distribution of these small-scale stresses are non-symmetric (they are limited by 0 on one side) and are skewed toward large values. These results constitute another validation of the numerical framework as the distribution reduces to a single point equal to the large-

scale values prescribed at the boundaries as Δx tends toward the horizontal dimension of the domain.

6.2 Experiments with an idealized ship

In a second set of experiments, we investigate the small-scale pressure field in the vicinity of a ship in heavy sea ice conditions and under compressive stresses. Importantly, we estimate the maximum pressure applied on the ship in different idealized experiments. The small-scale pressure field around a ship 90 m long and 30 m wide is investigated. We assume that the ship was navigating in level ice 2 m thick and that it is now beset. First, it is assumed that a lead (i.e., a channel) created by the ship is still open behind it over a distance of 600 m while further away the lead has been closed due to resulting sea ice convergence. The pressure field for this experiment is shown in Fig. 9a and with more details in Fig. 9b. Similar to our previous results without a ship, larger pressures are found at the tips of the lead. In fact, there are very large pressure on both sides of the ship, especially at the back of the ship. Numerical simulations of ships navigating in sea ice show larger pressure at the front of the ship (e.g. Kubat et al. (2010); Sayed et al. (2017)). However, our results show the opposite for a ship that is beset. These results also suggest that by navigating in these compact ice conditions, the ship has generated these high pressure conditions by creating a lead in its wake.

A crucial aspect to consider here is the length of the lead behind the ship. Assuming the leads closes at a shorter distance from the ship should imply smaller pressure values (for the same pressure applied at the boundaries). This is indeed the case as ~~it is~~ demonstrated by the sensitivity study shown in Fig. 10 ~~a. However, Fig. 10a~~ (blue curve)~~shows that even a small opening behind the ship leads to pressure values notably larger than the value prescribed at the boundaries. With only one grid cell (10 m) opened behind the ship, the pressure is ~2.5 times the value prescribed at the boundaries.~~ . We also consider the case of a lead partially consolidated. In fact, we assume that the concentration (A) is 0 just behind the ship and that it increases linearly to 1.0 for a certain lead length. The (mean) thickness h of the ice is set equal to Ah_l. This appears to have a very small effect on our results (not shown) compared to the case with A=0 everywhere in the lead (blue curve in Fig. 10~~a~~). This is due to the fact that the ice strength (see equation (7)) decreases rapidly as A diminishes. However, if we consider that the ice in the lead is consolidating through thermodynamical growth (i.e., we set h to a small value in the lead behind the ship) we find that this notably reduces the stress applied on the ship. This can be seen with the orange and magenta curves in Fig. 10 ~~a~~ which respectively correspond to thicknesses of 0.1 m and 0.2 m for the refrozen lead.

~~The results above were obtained by assuming certain mechanical characteristics for the ship (compressive and shear strengths). It is physically realistic to consider large compressive and shear strengths for the structure of the ship. However,~~ Fig. 10 shows that, for a certain large-scale pressure applied at the boundaries, the length of the lead behind the ship has a strong impact on the maximum pressure applied on the ship. Even though it is unclear ~~what shear strength should be used for the contour of the ship (related to ice-ship interactions). Given level ice of thickness~~ how long should be the lead for a given h_l ~~around the ship, we can reasonably assume that the shear strength for the contour of the ship has to be smaller than the shear strength~~

~~of this level ice~~ and for a given large-scale pressure, it is realistic to suppose that the higher the pressure at the boundaries, the shorter is the lead (i.e., it has closed over a certain distance due to the compressive stresses). Note that this is what is usually assumed for ships navigating in sea ice under compressive stresses (see for example Suominen and Kujala (2012)). In this last experiment, with results shown in Fig. 11, it is therefore assumed that the lead is 600 m long when the pressure at the boundaries is 0 kNm^{-1} and that it decreases linearly to 0 m when the pressure reaches 20 kNm^{-1} (blue curve) or when it reaches 15 kNm^{-1} (magenta curve). The relation between the lead length L and the pressure at the boundaries p_b is therefore $L = -30p_b + 600$ for the blue curve and $L = -40p_b + 600$ for the magenta one. We therefore consider here that the lead has consolidated mechanically and that there is no thermodynamical growth. Fig. 11 roughly exhibits three different regimes. In the first regime, for small pressure at the boundaries (i.e., ~~$P^* h_l/2e$).~~

~~Fig. 10b shows the results of a sensitivity study of the mechanical parameters for the ship.The maximum pressure applied on the ship is more sensitive to β (associated with the compressive strength~~ long lead length), the maximum pressure on the ship is linearly related to p_b because it is independent of lead length. In the second regime, for large pressure at the boundaries (i.e., small lead length), the maximum pressure is most sensitive to the lead length and we see again a linear dependence, with a negative slope, on p_b. In between, in the third regime, two compensating effects are playing out: a larger pressure at the boundaries causes the lead to be shorter which decreases the stress concentration in the vicinity of the ship~~) than it is to κ (associated with the shear strength of ship-ice interactions).See section ?? for details about κ and β.~~, making the maximum pressure weakly sensitive to the pressure at the boundary.

7 Conclusions

We have investigated how sea ice pressure could be downscaled at scales relevant for navigation. The distribution of pressure at small-scales is associated with non-uniform sea ice conditions. The PDF of the small-scale pressure is non-symmetric (it is limited by 0 on one side) and is skewed toward large values. Our results indicate that what really determines the largest values of pressure is associated with defects, that is long leads. Because a lead itself is not able to sustain any stress (unless it has refrozen), the load is taken by the ice around the lead with especially large values of the stresses in the vicinity of the tips. A sensitivity study indicates that the small-scale distribution and maximum pressure are notably affected by the choice of the shear strength (e) and compressive strength (P^*) for the elliptical yield curve. This suggests that a different yield curve and different mechanical strength properties would also lead to significantly different results.

Idealized experiments with a digitized ship beset in heavy sea ice conditions show that stress concentration also occurs in the vicinity of the ship. In fact, our simulations show that the largest pressure applied on the ship is found on both sides at the back of the ship. These results are different than the ones of Kubat et al. (2010) and Sayed et al. (2017) because our idealized ship is beset while they considered a digitized ship progressing in looser ice conditions.

We also argue that the ship itself is responsible for the strong concentration of stress on its side; the lead (or channel) it created by navigating in sea ice causes these large values of the stresses. Moreover, it is found that even a short lead causes pressure values notably larger than the pressure applied at the domain boundaries. The stresses on the ship should decrease as the ice in the lead consolidates (either by thermodynamical growth or closing of the lead). These conclusions highlight the difficulty of providing sub-grid scale pressure forecasts for navigation applications as the important parameters (i.e. the length of the lead and the thickness of the refrozen ice) are not well constrained.

A significant advantage of our numerical framework is that stresses can be specified at the boundaries. However, it is also important to note its limitations. First, it can only calculate the pressure field for a ship beset in heavy sea ice conditions; it cannot simulate the sea ice stresses applied on a ship navigating in ice infested waters (as in Kubat et al. (2010)). Also, in reality, sea ice convergence can cause ridging which can locally increase the yield strength of the ice. This strain hardening process was not considered in our numerical experiments; the maximum possible pressure in the domain is equal to $P^* h_l$. ~~Finally, a~~ Another possible limitation of our numerical framework is that the ice is modeled as a continuum material rather than a collection of discrete particles. It would be very interesting to still apply stresses at the boundaries but to model the interactions between the sea ice and the idealized ship with a model based on discrete floes (e.g., Daley et al. (2014); Metrikin and Løset (2013)).

In our numerical experiments, the digitized ship is simply represented as a rigid body with no outflow and no slip boundary conditions applied on the contour. A more realistic numerical framework should also involve a better representation of ship-ice interactions. For example, as done by Kubat et al. (2010), a Coulomb friction condition could be applied on the ship contour.

Although the convergence criterion for the steady-state solution of the velocity field has been reached in all the numerical experiments described in this paper, it is worth mentioning that this came with tremendous difficulties for the JFNK solver; the nonlinear convergence was really slow and the solver failed on some occasions to reach the required drop in the Euclidean norm of the residual within the allowed 500 nonlinear iterations. Lemieux et al. (2010) have already shown that the JFNK solver exhibits robustness issues as the grid is refined. In fact, it is really the number of unknowns that impacts the nonlinear convergence and robustness of the JFNK solver. This clearly indicates that innovations and more sophisticated numerical methods (e.g., Mehlmann and Richter (2017)) would be very beneficial for the sea ice modeling community.

Code availability. Revision 333 of the McGill sea ice model was modified so that stresses can be prescribed at the boundaries. This code is available on Zenodo at https://doi.org/10.5281/zenodo.3992822

Appendix A: Stability analysis

A few observations were made concerning the numerical stability of our new numerical framework with stresses applied at the boundaries. In this appendix, we discuss and provide explanations for these limitations.

1) We have noticed that for a simulation to be numerically stable, σ^W should be equal to σ^E, σ^S should be equal to σ^N and that all the shear stresses at the boundaries should have the same value (i.e., $\tau^W = \tau^E = \tau^S = \tau^N$). This can be easily understood by considering the ice in the domain as a single piece of ice. Assuming there is no shear stress, the sum of the forces applied on the ice along the x axis are

$$\sum F_x = \sigma^W \Delta x - \sigma^E \Delta x. \tag{A1}$$

For stability, $\sum F_x$ should be zero so that the ice does not accelerate indefinitely. This means that σ^W should be equal to σ^E. The same conclusion applies for σ^S and σ^N. Finally, a similar argument can be made for the shear stresses in terms of conservation of angular momentum. Interestingly, these conditions are the same ones found for the Cauchy tensor for the stresses at a point.

2) Dukowicz (1997) mentions, that for numerical stability, the internal stresses should be zero at open boundaries while our simulations show that it is possible to obtain stable solutions with non-zero stresses prescribed at the boundaries. To understand this, we revisit the stability analysis described in Dukowicz (1997). As Dukowicz (1997), we consider a simplified 1D momentum equation. However, we also take into account the replacement ~~pressure~~method. With these considerations, our 1D momentum equation is given by

$$\rho h \frac{\partial u}{\partial t} = \frac{\partial \sigma}{\partial x}, \tag{A2}$$

For stability, the rheology term should dissipate kinetic energy (KE). To investigate this, we multiply equation ~~A2~~ (A2) by u and integrate it over the whole domain ($x = 0$, i.e. the west side and $x = L$, i.e. the east side of our domain).

$$\int_0^L u \rho h \frac{\partial u}{\partial t} dx = \int_0^L u \frac{\partial \sigma}{\partial x} dx, \tag{A3}$$

As advection and thermodynamics are not considered, the thickness field is constant in time and we can write

$$\int_0^L \frac{\partial}{\partial t} \left(\frac{\rho h u^2}{2} \right) dx = \int_0^L u \frac{\partial \sigma}{\partial x} dx, \tag{A4}$$

In 1D, $\sigma = \alpha^2 \zeta \dot{\epsilon}_I - \zeta \Delta$ with $\zeta = \frac{P_p}{2\Delta^*}$, $\Delta^* = \min(\Delta, \Delta_{min})$, $\dot{\epsilon}_I = \frac{\partial u}{\partial x}$ and $\Delta = \alpha |\dot{\epsilon}_I|$ with $\alpha = \sqrt{1 + e^{-2}}$.

The term on the right can be integrated by parts, that is

$$\int_0^L u \frac{\partial \sigma}{\partial x} dx = [u\sigma]_0^L - \int_0^L \frac{\partial u}{\partial x} \sigma dx, \tag{A5}$$

$$\frac{\partial}{\partial t} \int_0^L \left(\frac{\rho h u^2}{2} \right) dx = u_L \sigma_L - u_0 \sigma_0 - \int_0^L \left(\alpha^2 \zeta \dot{\epsilon}_I^2 - \dot{\epsilon}_I \zeta \Delta \right) dx, \tag{A6}$$

where the time derivative has been moved outside the integral because the region of integration is fixed (Dukowicz, 1997). Note that $u_L = u|_{x=L}$ (same idea for the other terms). The term in the integral on the left is the total KE. From our results above we know that σ_L has to be equal to σ_0. By symmetry, we can also assume that $u_L = -u_0$. Hence, with the definition of the viscous coefficient, we can then write equation A6 as

$$\frac{\partial}{\partial t} KE = -2 u_0 \sigma_0 - \int_0^L \frac{\alpha P_p}{2\Delta^*} \left(\alpha \dot{\epsilon}_I^2 - \dot{\epsilon}_I |\dot{\epsilon}_I| \right) dx. \tag{A7}$$

For the second term on the right, $\left(\alpha \dot{\epsilon}_I^2 - \dot{\epsilon}_I |\dot{\epsilon}_I| \right) = \dot{\epsilon}_I^2 (\alpha - 1)$ if $\dot{\epsilon}_I$ is positive (divergence), while it is equal to $\dot{\epsilon}_I^2 (\alpha + 1)$ if $\dot{\epsilon}_I$ is negative (convergence). As $\alpha \geq 1$, this means that the integral is always positive and the term therefore always dissipates KE because of the minus sign in front of it. As opposed to the derivation of Dukowicz (1997), the replacement ~~pressure~~ method is also considered here. Nevertheless, consistent with his results, we find that the second term on the right always dissipates KE.

The stability therefore depends on the boundary term $-2u_0\sigma_0$. The worst condition happens when there is strong convergence at the boundaries. In this case, $\sigma_0 = -|\sigma_0| < 0$ and $u_0 > 0$ such that $2u_0|\sigma_0|$ is a source of KE. For a large convergence, we assume that the ice is in the plastic regime. To be able to evaluate the integral on the right in equation ~~A7~~(A7), we also look at a simple case with P_p that is constant over the whole domain. With these assumptions we find:

$$\frac{\partial}{\partial t} KE = 2 u_0 |\sigma_0| - \frac{\alpha P_p}{2} \int_0^L \frac{\dot{\epsilon}_I^2}{|\dot{\epsilon}_I|} dx + \frac{P_p}{2} \int_0^L \dot{\epsilon}_I dx. \tag{A8}$$

With $\dot{\epsilon}_I^2 / |\dot{\epsilon}_I| = |\dot{\epsilon}_I| = -\dot{\epsilon}_I$ because $\dot{\epsilon}_I < 0$ we can then write

$$\frac{\partial}{\partial t} KE = 2 u_0 |\sigma_0| + \frac{\alpha P_p}{2} \int_0^L \dot{\epsilon}_I dx + \frac{P_p}{2} \int_0^L \dot{\epsilon}_I dx. \tag{A9}$$

With $\int_0^L \dot{\epsilon}_I dx = \int_0^L \frac{\partial u}{\partial x} dx = u_L - u_0 = -2u_0$ we obtain

$$\frac{\partial}{\partial t} KE = 2u_0|\sigma_0| - (\alpha+1)P_p u_0. \tag{A10}$$

This means that $|\sigma_0|$ should be smaller that the compressive strength $(\alpha+1)P_p/2$ for the solution to be stable (i.e., the rheology term dissipates KE). A similar analysis can be conducted if we assume a tensile stress at the boundaries. In this case, we find that the stress $|\sigma_0|$ at the boundaries should be smaller than the tensile strength $(\alpha-1)P_p/2$.

To ensure numerical stability, Dukowicz (1997) mentions that the stresses should be zero at the open boundaries. This is a stricter condition that the one we find here. We have indeed demonstrated that the solution is stable as long as the stresses prescribed at the boundaries are between the compressive and tensile strengths of the ice. Numerical experiments (in 2D) confirm this finding. For example, when prescribing normal stresses of -10 kNm^{-1} on a uniform sea ice cover, the solution is stable if $h_l > 10$ kNm$^{-1}/P^*$ (not shown).

~~Notice that, to base our stability analysis on the KE energy, the term $\rho h \partial u/\partial t$ had to be included. This is different than the problem that is solved in our numerical experiments (i.e., $\nabla \cdot \sigma = 0$). We have, however, verified that the same numerical solutions can be obtained by finding the steady-state solution of $\rho h \frac{\partial u}{\partial t} = \nabla \cdot \sigma$.~~

Author contributions. JFL and BT developed the downscaling method and the modified boundary conditions. JFL modified the model code and conducted the numerical simulations. JFL, BT and MP analyzed and discussed the results. JFL wrote the manuscript with contributions from BT and MP.

Competing interests. The authors declare no competing interest.

Acknowledgements. We thank ~~Philippe~~ P. Blain for his comments and for carefully reading the manuscript. We also thank R. Frederking, H. Heorton and an anonymous reviewer for their very helpful comments. B. Tremblay would like to acknowledge the support of an NSERC-Discovery grant. Finally, we would like to thank F. Labelle and B. Niraula for developing the python code for Figure 1.

References

Bouchat, A. and Tremblay, B.: Using sea-ice deformation fields to constrain the mechanical strength parameters of geophysical sea ice, J. Geophys. Res. Oceans, 122, 5802–5825, https://doi.org/10.1002/2017JC013020, 2017.

Coon, M. D., Maykut, G. A., Pritchard, R. S., Rothrock, D. A., and Thorndike, A. S.: Modeling the pack ice as an elastic-plastic material, AIDJEX Bulletin, 24, 1–105, 1974.

Daley, C., Alawneh, S., Peters, D., and Colbourne, B.: GPU-Event-Mechanics Evaluation of Ice Impact Load Statistics, in: OTC Arctic Technology Conference, https://doi.org/10.4043/24645-MS, 2014.

Dukowicz, J. K.: Comments on the "stability of the viscous-plastic sea ice rheology", J. Phys. Oceanogr., 27, 480–481, 1997.

Dupont, F., Higginson, S., Bourdallé-Badie, R., Lu, Y., Roy, F., Smith, G. C., Lemieux, J.-F., Garric, G., and Davidson, F.: A high-resolution ocean and sea-ice modelling system for the Arctic and the North Atlantic oceans, Geosci. Model Dev., 8, 1577–1594, https://doi.org/10.5194/gmd-8-1577-2015, 2015.

Hebert, D. A., Allard, R. A., Metzger, E. J., Posey, P. G., Preller, R. H., Wallcraft, A. J., Phelps, M. W., and Smedstad, O. M.: Short-term sea ice forecasting: an assessment of ice concentration and ice drift forecasts using the U.S. Navy's Arctic cap nowcast/forecast system, J. Geophys. Res. Oceans, 120, https://doi.org/https://doi.org/10.1002/2015JC011283, 2015.

Heorton, H., Feltham, D., and Tsamados, M.: Stress and deformation characteristics of sea ice in a high-resolution, anisotropic sea ice model., Phil. Trans. R. Soc. A, 376, https://doi.org/http://dx.doi.org/10.1098/rsta.2017.0349, 2018.

Hibler, W. D.: A dynamic thermodynamic sea ice model, J. Phys. Oceanogr., 9, 815–846, 1979.

Hutchings, J. K., Heil, P., and Hibler, W. D.: Modeling linear kinematic features in sea ice, Mon. Wea. Rev., 133, 3481–3497, 2005.

Jeong, S.-Y., Choi, K., Kang, K.-J., and Ha, J.-S.: Prediction of ship resistance in level ice based on empirical approach, International Journal of Naval Architecture and Ocean Engineering, 9, 613 – 623, https://doi.org/https://doi.org/10.1016/j.ijnaoe.2017.03.007, http://www.sciencedirect.com/science/article/pii/S2092678215300066, 2017.

Kreyscher, M., Harder, M., Lemke, P., and Flato, G. M.: Results of the Sea Ice Model Intercomparison Project: Evaluation of sea ice rheology schemes for use in climate simulations, J. Geophys. Res., 105, 11 299–11 320, 2000.

Kubat, I., Sayed, M., and Collins, A.: Modeling of pressured ice interaction with ships, in: Transactions - Society of Naval Architects and Marine Engineers, Paper No. ICETECH10-138-R0, 2010.

Kubat, I., Babaei, M., and Sayed, M.: Quantifying ice pressure conditions and predicting the risk of ship besetting, in: Transactions - Society of Naval Architects and Marine Engineers, Paper No. ICETECH12-130-RF, 2012.

Kubat, I., Sayed, M., and Babaei, M.: Analysis of besetting incidents in Frobisher Bay during 2012 shipping season, in: Proceedings of the 22nd International conference on port and ocean engineering under Arctic conditions, 2013.

Kulaots, R., Kujala, P., von Bock und Polach, R., and Montewka, J.: Modelling of ship resistance in compressive ice channels, in: POAC 13: Proceedings of the 22^{nd} International Conference on Port and Ocean Engineering under Arctic Conditions, 2013.

Leisti, H., Kaups, K., Lehtiranta, J., Lindfors, M., Suominen, M., Lensu, M., Haapala, J., Riska, K., and Kouts, T.: Observations of ships in compressive ice., Proceedings of the 21^{st} international conference on Ports and Ocean Engineering under Arctic Conditions, 2011.

Lemieux, J.-F. and Tremblay, B.: Numerical convergence of viscous-plastic sea ice models, J. Geophys. Res., 114, C05 009, https://doi.org/10.1029/2008JC005017, 2009.

Lemieux, J.-F., Tremblay, B., Sedláček, J., Tupper, P., Thomas, S., Huard, D., and Auclair, J.-P.: Improving the numerical convergence of viscous-plastic sea ice models with the Jacobian-free Newton Krylov method, J. Comput. Phys., 229, 2840–2852, https://doi.org/10.1016/j.jcp.2009.12.011, 2010.

Lemieux, J.-F., Knoll, D. A., Losch, M., and Girard, C.: A second-order accurate in time IMplicit-EXplicit (IMEX) integration scheme for sea ice dynamics, J. Comput. Phys., 263, 375–392, https://doi.org/10.1016/j.jcp.2014.01.010, 2014.

Lindqvist, G.: A straightforward method for calculation of ice resistance of ships, in: Proceedings of the 10th International Conference on Port and Ocean Engineering under Arctic Conditions (POAC), pp. 722–735, 1989.

Lubbad, R. and Loset, S.: A numerical model for real-time simulation of ship-ice interaction, Cold Reg. Sci. Technol., 65, 111–127, https://doi.org/https://doi.org/10.1016/j.coldregions.2010.09.004, 2011.

Mehlmann, C. and Richter, T.: A modified global Newton solver for viscous-plastic sea ice models, Ocean Modelling, 116, 96 – 107, https://doi.org/https://doi.org/10.1016/j.ocemod.2017.06.001, http://www.sciencedirect.com/science/article/pii/S1463500317300902, 2017.

Metrikin, I. and Løset, S.: Nonsmooth 3D Discrete Element Simulation of a Drillship in Discontinuous Ice, in: POAC 13: Proceedings of the 22^{nd} International Conference on Port and Ocean Engineering under Arctic Conditions, 2013.

Montewka, J., Goerlandt, F., Kujala, P., and Lensu, M.: Towards probabilistic models for the prediction of ship performance in dynamic ice, Cold Reg. Sci. Technol., 112, 14–28, 2015.

Mussells, O., Dawson, J., and Howell, S.: Navigating pressured ice: Risks and hazards for winter resource-based shipping in the Canadian Arctic, Ocean & Coastal Management, 137, 57 – 67, https://doi.org/https://doi.org/10.1016/j.ocecoaman.2016.12.010, http://www.sciencedirect.com/science/article/pii/S0964569116303969, 2017.

Ringeisen, D., Losch, M., Tremblay, L., and Hutter, N.: Simulating intersection angles between conjugate faults in sea ice with different viscous–plastic rheologies, The Cryosphere, 13, 1167–1186, https://doi.org/https://doi.org/10.5194/tc-13-1167-2019, 2019.

Sayed, M., Islam, S., Watson, D., Kubat, I., Gash, R., and Wright, B.: DP Drillship Stationkeeping in Ice - Comparison Between Numerical Simulations and Ice Basin Tests, in: The 27^{th} International Ocean and Polar Engineering Conference, 2017.

Su, B., Riska, K., and Moan, T.: A numerical method for the prediction of ship performance in level ice, Cold Regions Science and Technology, 60, 177 – 188, https://doi.org/https://doi.org/10.1016/j.coldregions.2009.11.006, http://www.sciencedirect.com/science/article/pii/S0165232X09002092, 2010.

Suominen, M. and Kujala, P.: Ice model tests in compressive ice, in: Proceedings of the 21^{st} IAHR International Symposium on Ice "Ice Research for a Sustainable Environment", 2012.

Turnbull, I. D., Bourbonnais, P., and Taylor, R. S.: Investigation of two pack ice besetting events on the Umiak I and development of a probabilistic prediction model, Ocean Eng., 179, 79–91, https://doi.org/https://doi.org/10.1016/j.oceaneng.2019.03.030, 2019.

Williams, J. and Tremblay, L. B.: The dependence of energy dissipation on spatial resolution in a viscous-plastic sea-ice model, Ocean Modelling, 130, 40–47, https://doi.org/https://doi.org/10.1016/j.ocemod.2018.08.001, 2018.

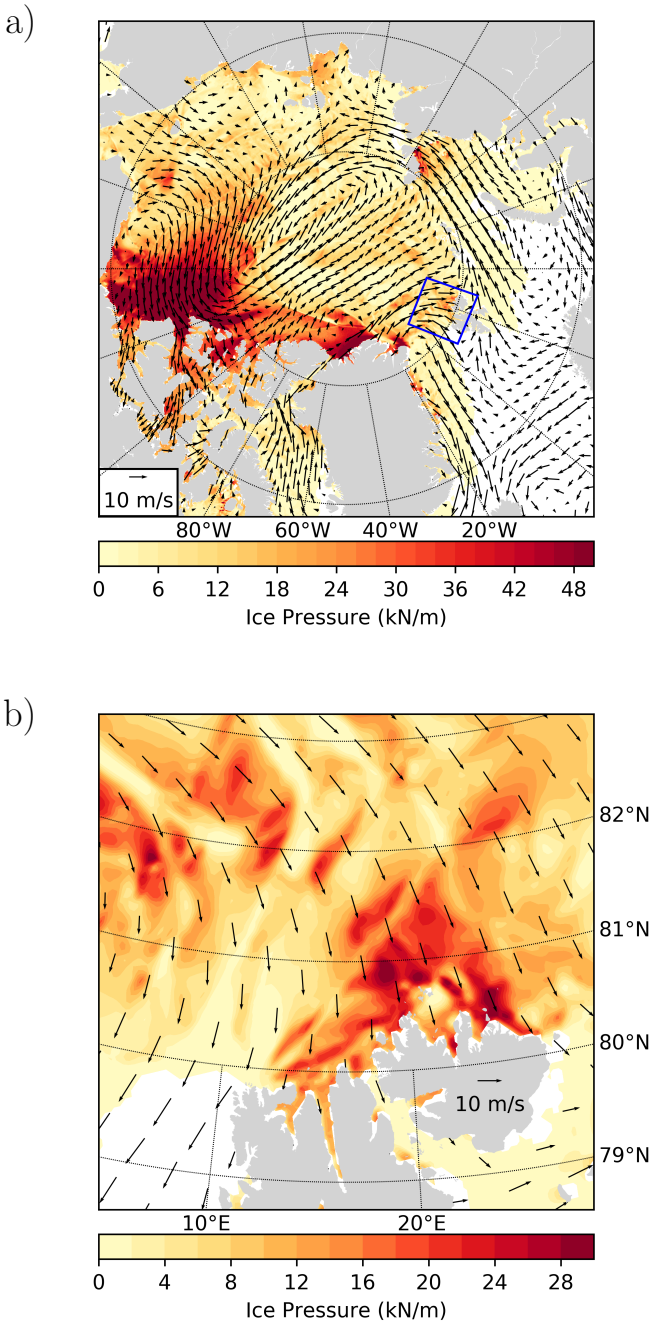

Figure 1. 24 h forecast of the sea ice pressure (kNm^{-1}) and of the surface winds (ms^{-1}) from the Canadian Arctic Prediction System (CAPS). The forecast was initiated at 00 UTC on 29 April 2020. Almost all of the domain is shown in panel a) while panel b) is a subset of the domain located in the region of Svalbard (the sub-region is defined by the blue rectangle in panel a). Note that the color scale is not the same for the two panels.

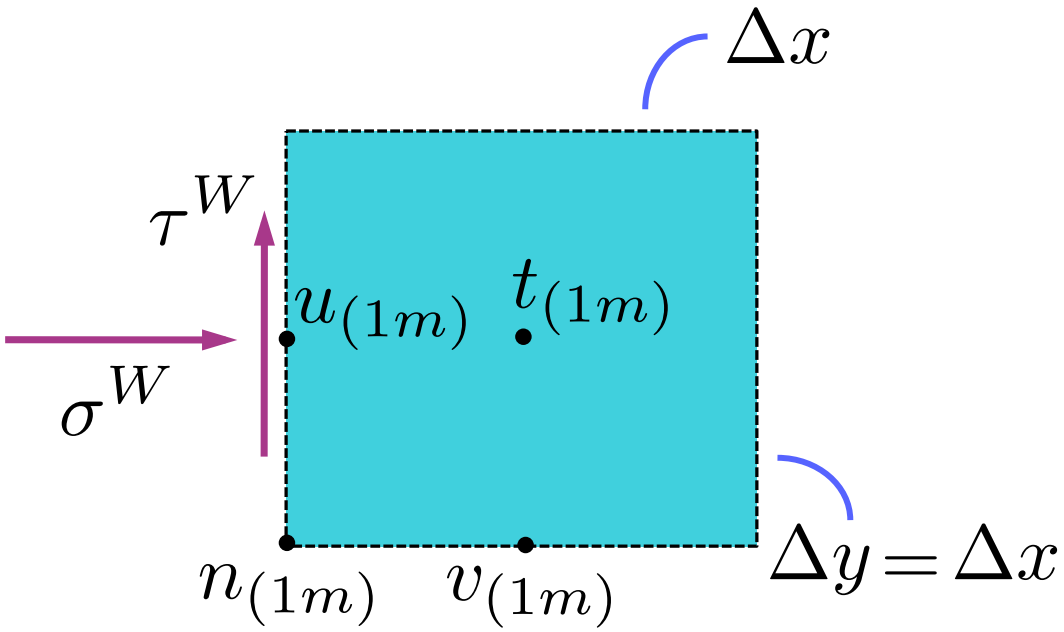

Figure 2. One grid cell on the western boundary of the domain with indices $l = 1$ and m. This figure shows the location of the velocity components on the C-grid of the McGill model. The variables h and A are positioned at the tracer point t. Some variables (e.g. σ_{12}) are also calculated at the node (n) point. The stresses (σ^W and τ^W) applied at the western boundary are shown with purple arrows.

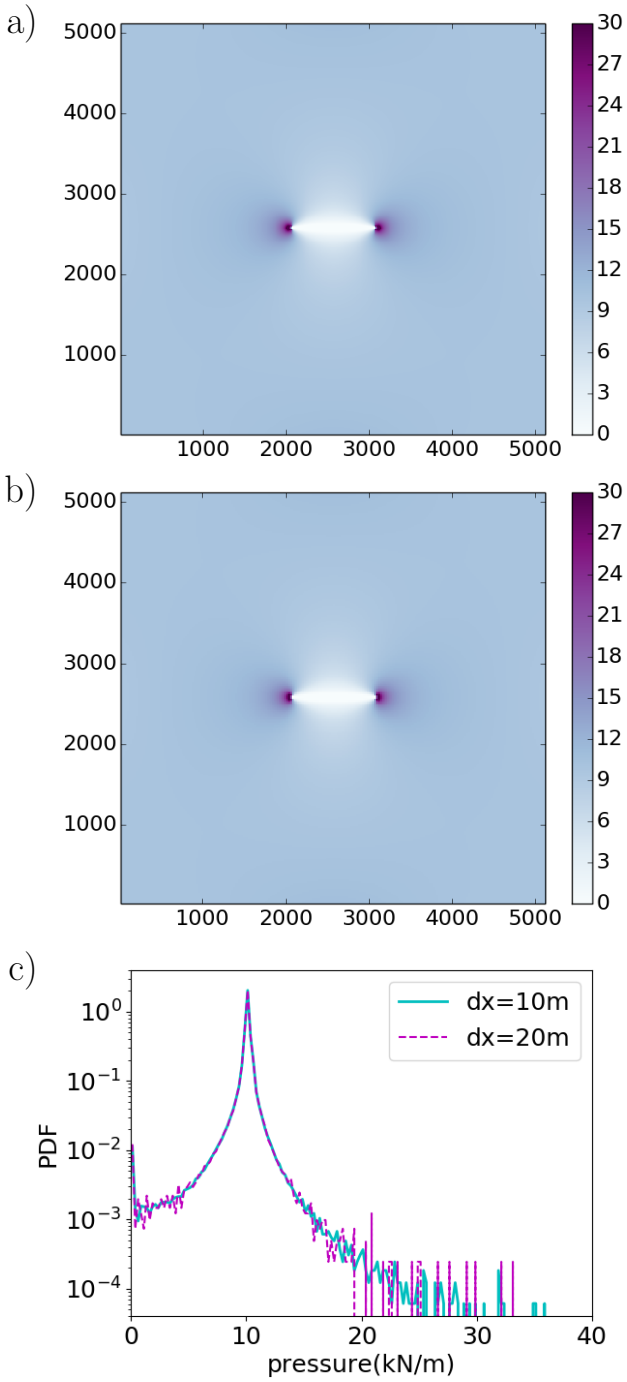

Figure 3. Pressure field for Δx =10 m (a) and Δx =20 m (b). The thickness field is 2 m everywhere except a 1 km long, 40 m wide horizontal lead in the middle of the domain. The normal stresses at the boundaries are -10 kNm^{-1}. The last panel (c) shows PDFs of the pressure in the 5×5 km domain for Δx =10 m (cyan) and Δx =20 m (magenta). Bins of 0.25 kNm^{-1} were used to build the PDFs.

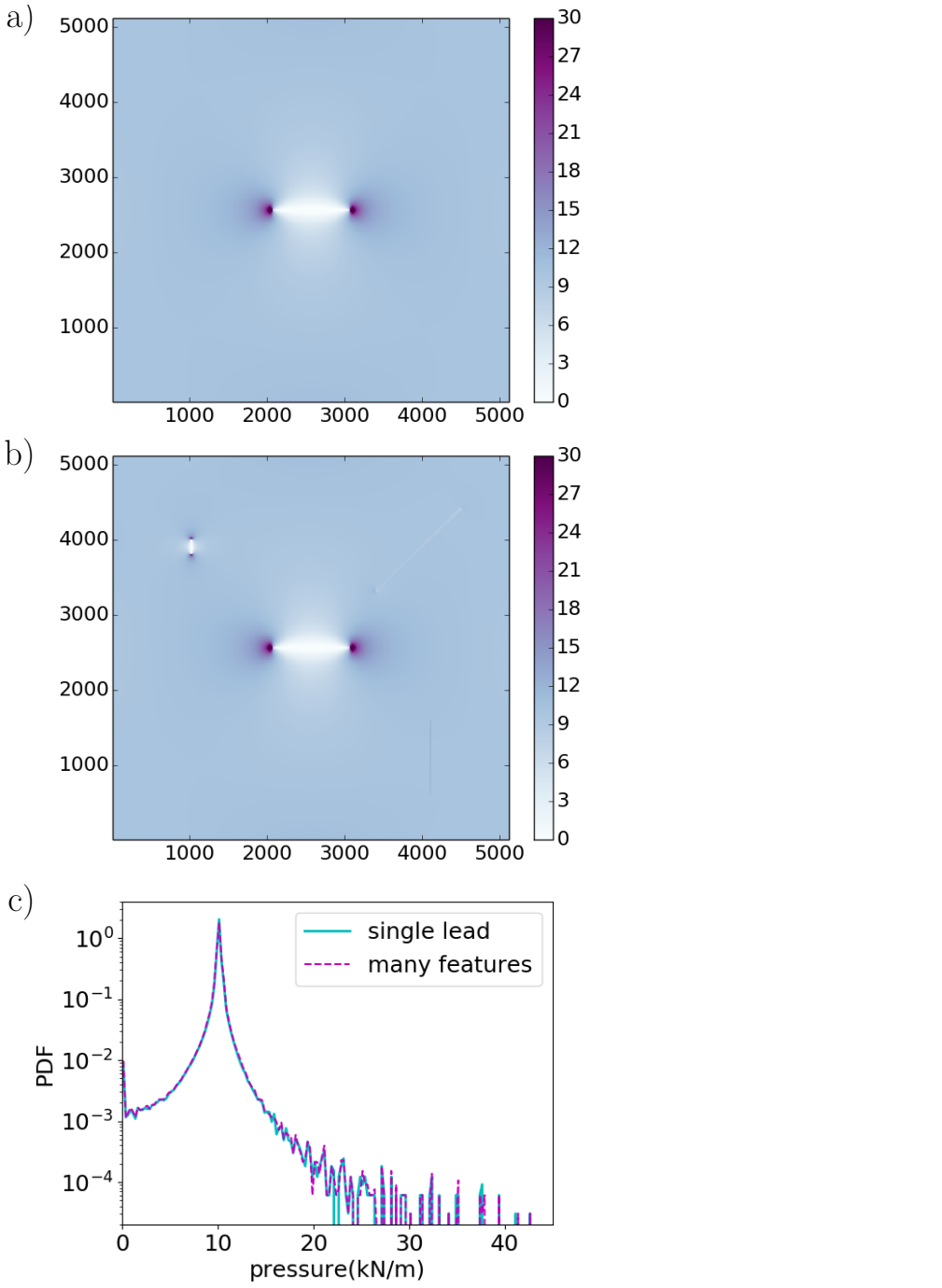

Figure 4. Pressure (kNm^{-1}) field for a thickness field of 2 m everywhere except a 1 km long, 10 m wide horizontal lead in the middle of the domain (a, referred to as 'single lead'). Pressure (kNm^{-1}) field for a thickness field of 2 m everywhere except a 1 km long, 10 m wide horizontal lead in the middle of the domain, a diagonal refrozen lead (h=0.5m), a smaller lead in the northwestern part of the domain and a 1 km ridge (max h = 5 m in center, 2.5 m on each side) in the southeastern part of the domain (b, referred to as 'many features'). For both experiments $\Delta x = 10$ m and the normal stresses at the boundaries are -10 kNm^{-1}. PDFs of the pressure for the 'single lead' experiment (cyan) and the 'many features' experiment (dashed magenta)

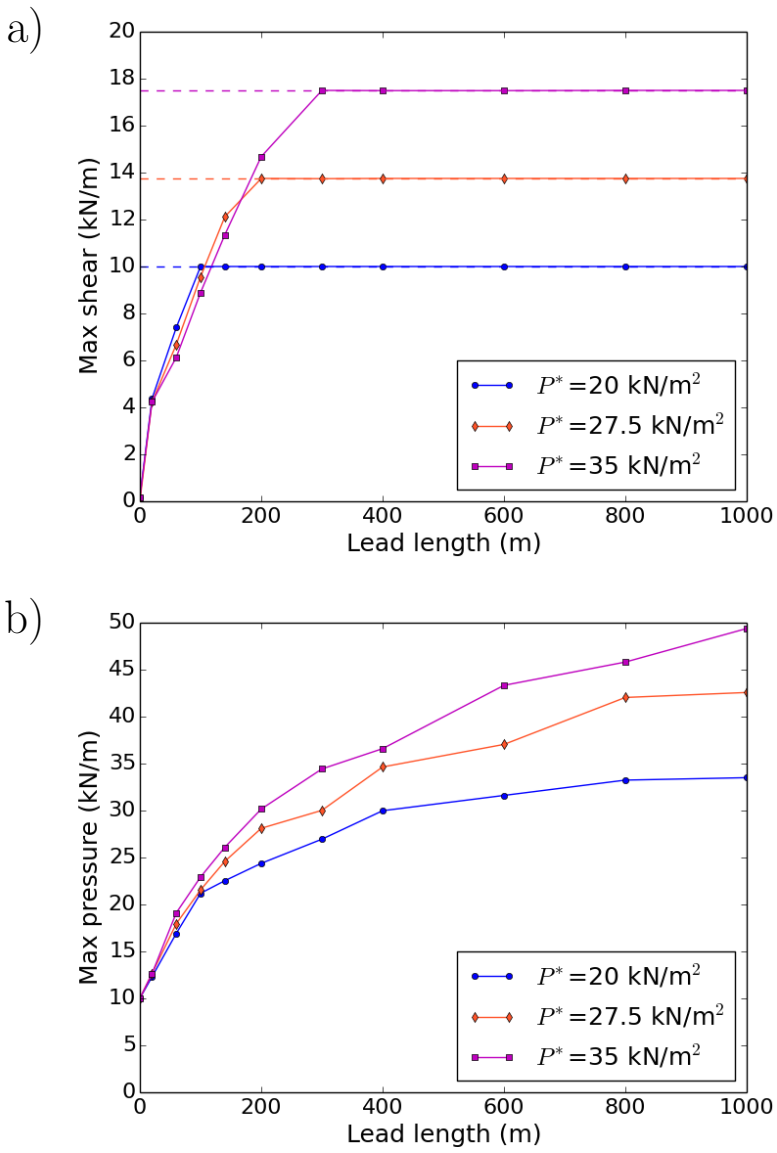

Figure 5. Maximum value of the shear stress invariant (a, kNm^{-1}) and of the pressure (b, kNm^{-1}) in the domain as a function of lead length for different values of the parameter P^* (P^*=20 kNm^{-2}: blue, P^*=27.5 kNm^{-2}: orange, P^*=35 kNm^{-2}: magenta). The thickness field is 2 m everywhere except the 10 m wide horizontal lead in the middle of the domain. The normal stresses at the boundaries are -10 kNm^{-1}.

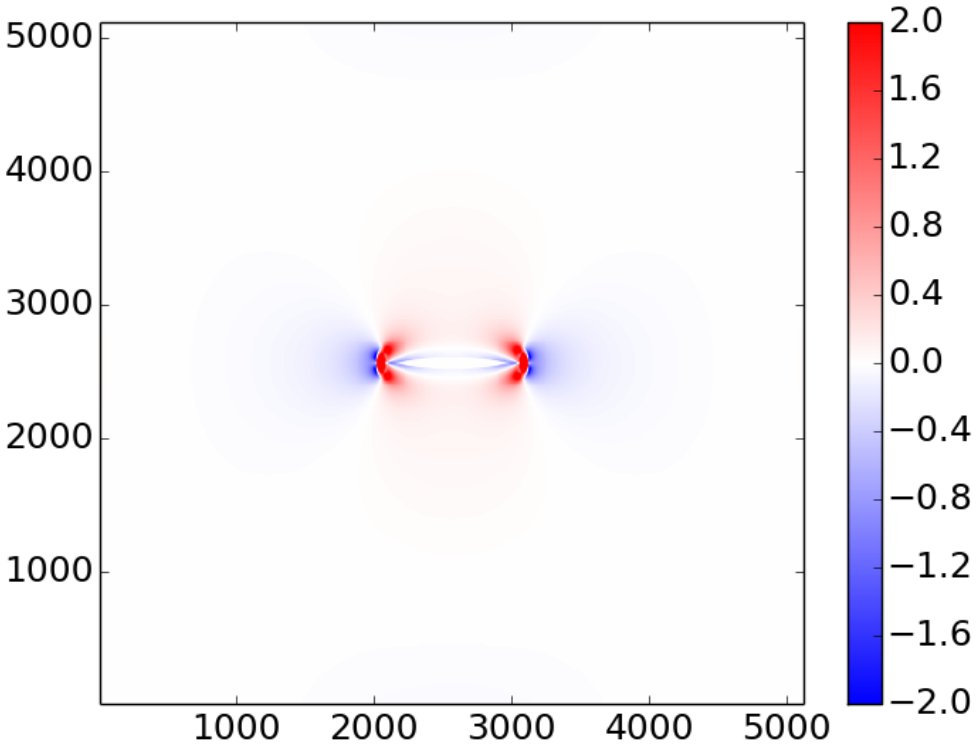

Figure 6. Pressure field with P^*=27.5 kNm^{-2} minus the pressure field with P^*=20.0 kNm^{-2} (in kNm^{-1}). For both experiments, the thickness field is 2 m everywhere except a 1 km long, 10 m wide horizontal lead in the middle of the domain. The normal stresses at the boundaries are -10 kNm^{-1}.

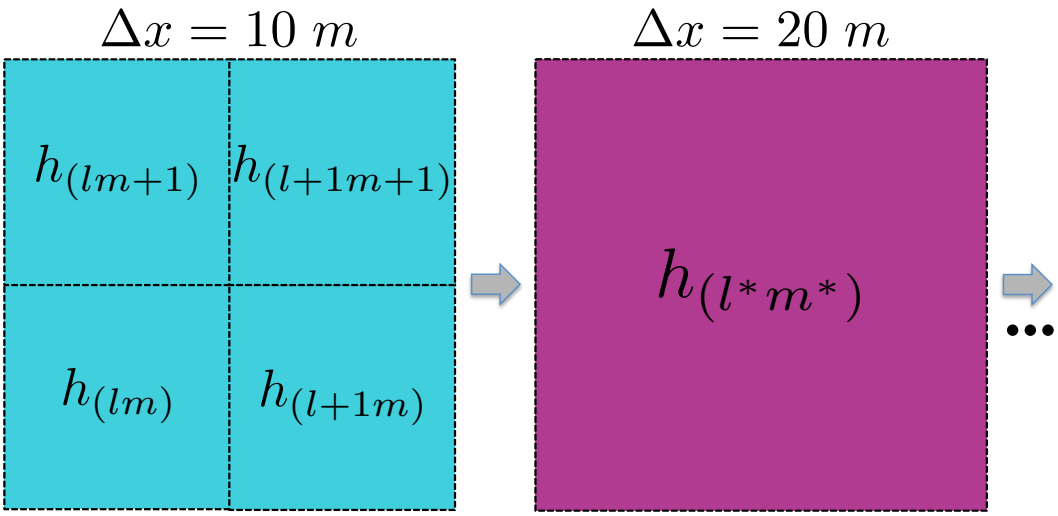

Figure 7. Schematic of the coarse-graining procedure. The thickness field is defined at 10 m resolution (blue cells on the left). The thickness field at 20 m resolution is obtained by averaging the h values of the four 10 m cells contained in the 20 m one (purple cell). This procedure is repeated for the other lower resolutions. The same method is applied for the concentration A. The indices l, m are for the 10 m grid while the indices l^*, m^* are for the 20 m grid.

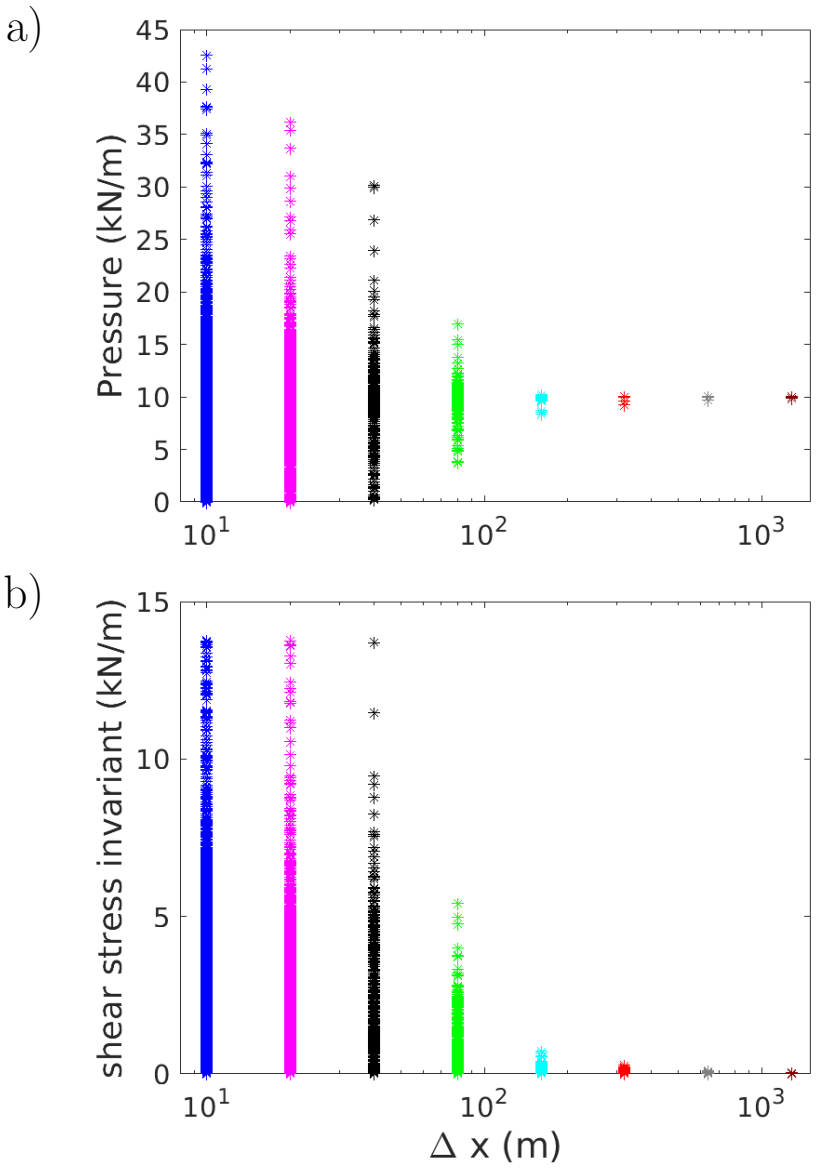

Figure 8. All the values of pressure (a) and of the shear stress invariant (b) in the 5×5 km domain as a function of resolution. The thickness field is 2 m everywhere except a 1 km long, 10 m wide horizontal lead in the middle of the domain. The initial thickness and concentration fields at the other resolutions are obtained through a coarse-graining procedure. The normal stresses at the boundaries are -10 kNm^{-1}.

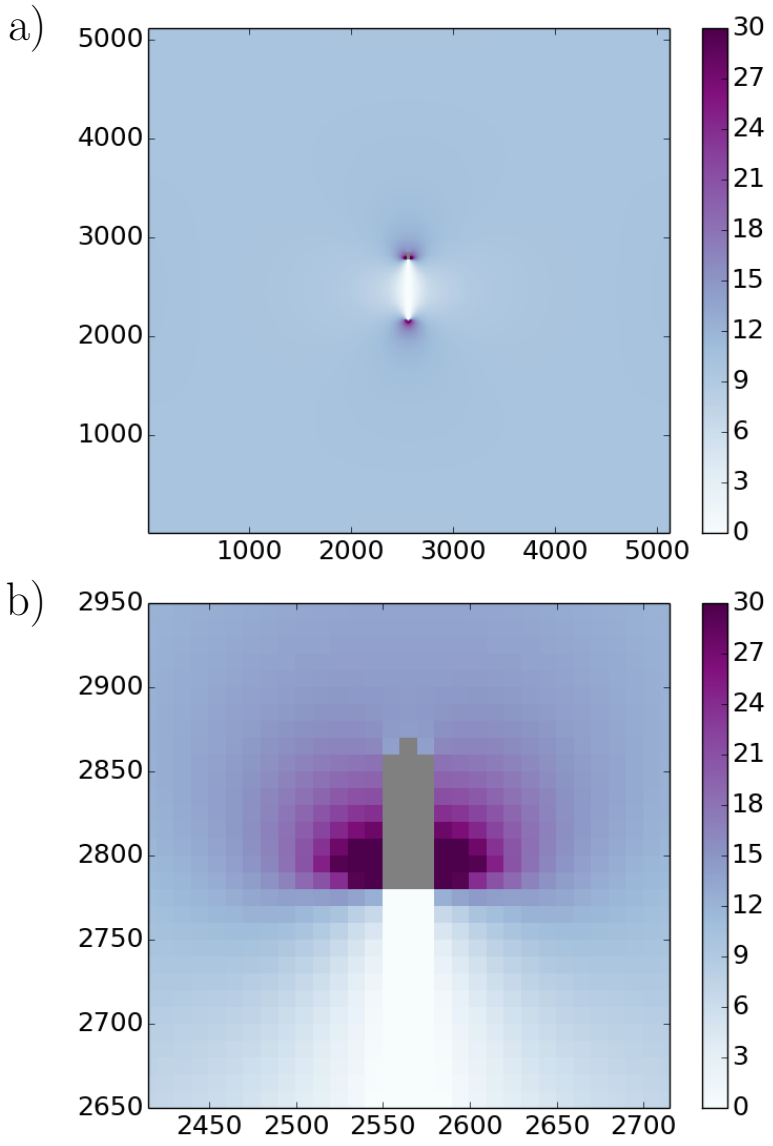

Figure 9. Pressure field at 10 m resolution when including a digitized ship 90 m long and 30 m wide (in gray). The thickness field is 2 m everywhere except a 600 m long lead behind the ship. The normal stresses at the boundaries are -10 kNm^{-1}. The whole domain is shown in panel a while panel b shows a zoom of the pressure field around the ship.

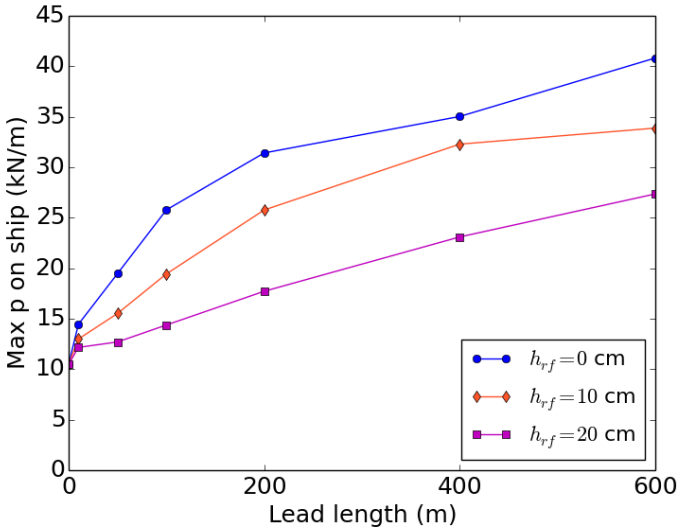

Figure 10. Maximum pressure (kNm^{-1}) on the ship as a function of the length of the lead behind the ship~~(a)~~. The thickness field is 2 m everywhere except in the lead behind the ship; ~~it~~ the thickness of the refrozen lead (h_{rf}) is 0 cm for the blue curve, it is 10 cm for the orange one and it is 20 cm for the magenta one. ~~Maximum pressure (kNm^{-1}) on the ship (b) as a function of the parameter κ for four different values of the β parameter (β=5: blue, β=10: orange, β=15: gray, β=20: magenta).~~ The ~~parameter κ defines the shear strength on the contour of the ship while β defines the strength in compression of the ship. The thickness field is 2 m everywhere except in the 200 m long lead behind the ship. The~~ digitized ship is 90 m long and 30 m wide. The normal stresses at the boundaries are -10 kNm^{-1}.

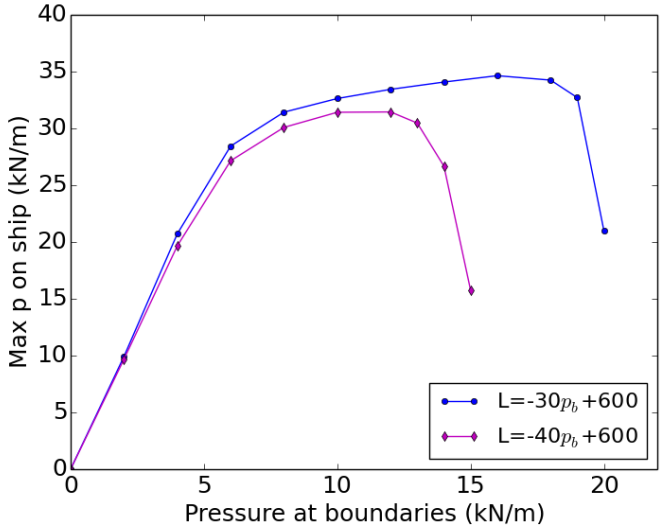

Figure 11. Maximum pressure (kNm^{-1}) on the ship as a function of the pressure (p_b) prescribed at the boundaries. For both curves, it is assumed that the length of the lead (L) is 600 m for p_b=0 kNm^{-1} and that it decreases linearly as p_b increases. For the blue, the lead behind the ship is closed when p_b reaches 20 kNm^{-1} while the lead is closed when p_b=15 kNm^{-1} for the magenta curve. The thickness field is 2 m everywhere except in the lead behind the ship where the thickness is 0 m. The digitized ship is 90 m long and 30 m wide.